



M Ű E G Y E T E M 1 7 8 2

BUDAPEST UNIVERSITY OF TECHNOLOGY AND ECONOMICS  
DEPARTMENT OF APPLIED MECHANICS



University of  
**BRISTOL**

UNIVERSITY OF BRISTOL  
DEPARTMENT OF ENGINEERING MATHEMATICS

# The effect of time delay in skateboard balancing

A thesis submitted for the degree of  
*Master of Science*

*Author:*

Balázs VÁRSZEGI

*Tutors:*

Dénes TAKÁCS, PhD<sup>(1)</sup>

Stephen John HOGAN, PhD<sup>(2)</sup>

<sup>(1)</sup> Budapest University of Technology and Economics  
Department of Applied Mechanics

<sup>(2)</sup> University of Bristol  
Department of Engineering Mathematics

2013, Budapest



## NYILATKOZAT

a  
szakdolgozat beadásához

Alulírott, VÁRSZEGI Balázs a Budapesti Műszaki és Gazdaságtudományi Egyetem Gépészmérnöki Karának gépészmérnöki mesterszakos végzős hallgatója nyilatkozom, hogy a *Az időkéleltetés szerepe a gördeszka egyensúlyozásában* címmel a 2013. évben írt és bírálatra, valamint védeésre beadott szakdolgozatom saját munkám eredménye, amelynek elkészítése során a felhasznált irodalmat a szerzői jogi szabályoknak megfelelően kezeltem (a szükséges lábjegyzet/végjegyzet hivatkozásokat, valamint az ábrák hivatkozását megfelelően helyeztem el).

Budapest, 2013. december 13.

VÁRSZEGI Balázs  
G2EVYZ

A hallgató aláírása

## Acknowledgements

During the period of my studies, I have had cause to be grateful for the advice, support and understanding of many people.

First of all, I would like to say special thanks to Dénes Takács, who was my tutor since the beginning of my BSc thesis work. His constant and invaluable scientific and personal support helped me considerably in my research. I also thank Professor John Hogan at University of Bristol, who hosted me during my time in Bristol and helped with my thesis work. I also thank to Professor Gábor Stépán (Budapest University of Technology and Economics) for useful advice and guidance.

Special thanks to my family and my girlfriend for their patience and support during my work, without these my thesis would not have been possible.

Finally I would like to thank to all of my friends for the refreshing times, that we spent together, especially the relaxing runs and conversations.

## Kivonat

### Az időkéleltetés szerepe a gördeszka egyensúlyozásában

*MSc Diplomateru*, készítő: Várszegi Balázs

Sokszor a legegyszerűbb közlekedési eszközeink is érdekes, nem várt instabilitásokat mutatnak. Például a járműdinamikában mindmáig kutatott a kerékpárok és gördeszkák lineáris stabilitása. Dolgozatom célja a gördeszka mozgásának leírása, illetve az egyenes vonalú egyenletes mozgás lineáris stabilitásvizsgálata.

A vizsgálatok elvégzéséhez elkészítettem a gördeszka legegyszerűbb mechanikai modelljét, amely csupán egy tömegpontot tartalmaz és két darab tömeg nélküli rudat, valamint egy torziós rugót, amely a gördeszka kormányzásáért felelős gumibakot modellezi. A gördeszka legalapvetőbb mechanikai modelljében is figyelembe kell vennünk a gördeszka irányítását meghatározó kinematikai kényszereket. Azaz, még a legegyszerűbb modell is anholonom rendszert alkot, mely rendszerek mozgásegyenleteit nem lehet a másodfajú Lagrange-egyenletekkel segítségével meghatározni. Így azok előállítására elsődlegesen az Appell-Gibbs-egyenleteket használtam.

A megalkotott mechanikai modell segítségével a gördeszka egyenes vonalú egyenletes mozgásának lineáris stabilitását vizsgáltam, valamint adtam egy áttekintő képet a modell nemlineáris viselkedéséről. Stabilitási térképeket készítettem a stabil és instabil sebességtartományok megjelenítéséhez. A modell hasonlóan viselkedik, mint egy torziós rugóval megtámasztott inverz inga, a stabilitási feltételek is hasonlóra adódnak, azzal a különbséggel, hogy a stabil egyenes vonalú egyenletes mozgáshoz szükséges rugómerevség nagysága a gördeszka sebességétől függ.

Ezek alapján megállapítható, hogy amennyiben az egyenes vonalú mozgás kis sebesség esetén instabil, akkor is lehet a gördeszka egyenes vonalú mozgása stabil nagyobb sebességek esetén. Hasonló megállapítások találhatók egy egyszerűsített biciklimodell vizsgálat tanulmányban, amelyben a számítások helyességét kísérletekkel is igazolták.

Mivel a vizsgált modellel nem lehet magyarázni a gördeszka nagyobb sebességnél fellépő stabilitásvesztését – amely jól ismert probléma a gyakorlott gördeszkások körében – ezért a modellt kiegészítettem egy szabályozási körrel, amely a gördeszkázó személy gördeszkára való hatását hivatott modellezni. A szabályozási körben figyelembe vettem a gördeszkás reakcióidejéből fakadó időkésést. A gördeszka stabilitását különböző sebességek és szabályozási paraméterek mellett vizsgáltam.

## Abstract

### The effect of time delay in skateboard balancing

*MSc Thesis* by Balázs Várszegi

The simplest vehicles sometimes show interesting unwanted instabilities. For example, even nowadays the linear stability of bicycles and skateboards is investigated even nowadays in several studies of vehicle dynamics. The goals of this study are the investigation of the motion of the skateboard and the stability analysis of its straight stationary motion.

We have constructed possibly the simplest model of the skateboard, which consists of a mass point, two massless rods and one torsion spring that models the rubber element in the wheel suspension system. Kinematic constraints play a key role in the motion of skateboard, thus, the simplest model has to consider them. Hence, the simplest model of the skateboard is nonholonomic, thus, the equations of motion of the system can not be derived with the help of the Lagrange equations of the second kind. Therefore, we derived the equations of motion by means of the Appell–Gibbs equations.

By means of the composed mechanical model, the linear stability of the straight stationary rolling is analyzed and we briefly consider the nonlinear behaviour. The system behaves like an inverted pendulum supported by a torsion spring; the stability criteria are also similar except that in the case of the skateboard the stability also depends on the speed. Based on our results, it can be established that the straight stationary rolling of the skateboard can be stable at great speed even if it is unstable at smaller speeds. Similar results are published about a simplified mechanical model of the bicycle, where experiments are also carried out in order to validate the theoretical analysis.

Since, the composed model is unable to show the well-known instability problem of skateboard at large speeds, the control loop of the rider was also considered in the mechanical model. The reaction time was implemented into the model by means of the time delay in the control. The stability of the skateboard was studied for different speeds and control parameters.

# Contents

<b>1</b>	<b>Introduction</b>	<b>1</b>
<b>2</b>	<b>The self-balancing skateboard</b>	<b>2</b>
2.1	Self-balancing skateboard . . . . .	2
2.1.1	Mechanical model . . . . .	2
2.1.2	Skater's state of motion . . . . .	5
2.1.3	Kinematic constraints . . . . .	6
2.1.4	Equation of motion . . . . .	7
2.1.5	Linear stability analysis of the straight line motion . . . . .	11
2.1.6	Nonlinear Analysis . . . . .	13
2.2	Nearly self-balancing skateboard . . . . .	15
2.2.1	Mechanical model . . . . .	15
2.2.2	Equation of motion . . . . .	16
2.2.3	Conservative quantity . . . . .	17
2.2.4	Linear stability analysis of the straight line motion . . . . .	18
2.2.5	Nonlinear analysis . . . . .	19
2.2.6	Limit cycle . . . . .	23
2.3	Comparing the models . . . . .	24
<b>3</b>	<b>Controlled skateboard</b>	<b>25</b>
3.1	Derivation of the equation of motion . . . . .	25
3.1.1	Mechanical model . . . . .	25
3.1.2	Equation of motion . . . . .	27
3.2	Rigid skater – board connection . . . . .	30
3.3	Simple skater balancing . . . . .	31
3.3.1	Equation of motion . . . . .	31
3.3.2	Linear stability analysis of the straight line motion . . . . .	32
3.4	Riding on skateboard with reflex time . . . . .	36

---

3.4.1	Equation of motion . . . . .	36
3.4.2	Linear stability analysis of the straight line motion . . . . .	37
<b>4</b>	<b>Summary</b>	<b>46</b>
	<b>Bibliography</b>	<b>47</b>
<b>A</b>	<b>Numerical simulations for the totally self-balancing skateboard</b>	<b>49</b>
<b>B</b>	<b>Phase-space for the non-conservative skateboard model</b>	<b>54</b>
<b>C</b>	<b>Numerical simulations for the nearly self-balancing skateboard</b>	<b>56</b>
<b>D</b>	<b>Numerical simulations for the PD controlled skateboard</b>	<b>61</b>
<b>E</b>	<b>Numerical simulations for the delayed PD controlled skateboard</b>	<b>67</b>

# List of Figures

2.1	Mechanical model of the self-balancing skateboard . . . . .	3
2.2	Suspension geometry . . . . .	4
2.3	Turning mechanism of skateboard . . . . .	4
2.4	Stability chart of the totally self-balancing skateboard . . . . .	13
2.5	Mechanical model of the nearly self-balancing skateboard . . . . .	15
2.6	Graphical solution for equilibria . . . . .	20
2.7	Different phase-space structures in the space of energy ratios . . . . .	21
2.8	Structure of phase-space in specific domains . . . . .	22
3.1	Mechanical model of the controlled skateboard . . . . .	26
3.2	Free-body diagram of the controlled skateboard model in $x - y$ plane . . . . .	28
3.3	Explanation for stability charts of the PD controlled skateboard in case of all the expressions (3.3.13) are less than zero . . . . .	33
3.4	Explanation for stability charts of the PD controlled skateboard in case of all the expressions (3.3.13) are greater than zero . . . . .	34
3.5	Stability charts of the PD controlled skateboard with the effect of changing the proportional parameter and the longitudinal velocity . . . . .	35
3.6	Number of positive solutions for $\tilde{\omega}$ (and also $\tilde{\omega}^2$ ) . . . . .	40
3.7	Structure of the stability chart of the PD controlled skateboard with the skater's reflex time . . . . .	41
3.8	Critical time delay . . . . .	42
3.9	Critical spring stiffness for stable domain . . . . .	43
3.10	Dimensionless stability charts of the PD controlled skateboard with the skater's reflex time . . . . .	44
3.11	Stability charts of the PD controlled skateboard with the skater's reflex time . . . . .	45
A.1	Numerical simulations for totally self-balancing skateboard in the stable case . . . . .	50
A.2	Numerical simulations for totally self-balancing skateboard in dynamically unstable case . . . . .	51

---

A.3	Numerical simulations for totally self-balancing skateboard in the statically unstable case . . . . .	52
A.4	Numerical simulations for the totally self-balancing skateboard with large perturbation . . . . .	53
B.1	Structure of phase-space for specific domains with a skater, who stands before the centre of the board . . . . .	54
B.2	Structure of phase-space for specific domains with a skater, who stands after the centre of the board . . . . .	55
C.1	Numerical simulations for nearly self-balancing skateboard in the stable case	57
C.2	Numerical simulations for nearly self-balancing skateboard in the dynamically unstable case . . . . .	58
C.3	Numerical simulations for nearly self-balancing skateboard in the statically unstable case . . . . .	59
C.4	Numerical simulations for nearly self-balancing skateboard with big perturbation . . . . .	60
D.1	Numerical simulations for PD controlled skateboard in the stable case with $P$ less than $P_c$ and negative $a$ . . . . .	62
D.2	Numerical simulations for PD controlled skateboard in the stable case with $P$ less than $P_c$ and positive $a$ . . . . .	63
D.3	Numerical simulations for PD controlled skateboard in the stable case with $P$ more than $P_c$ . . . . .	64
D.4	Numerical simulations for PD controlled skateboard in the unstable case with $P$ less than $P_c$ . . . . .	65
D.5	Numerical simulations for PD controlled skateboard in the unstable case with $P$ more than $P_c$ . . . . .	66
E.1	Numerical simulations for delayed PD controlled skateboard for the stable case . . . . .	68
E.2	Numerical simulations for delayed PD controlled skateboard for the statically unstable case . . . . .	69
E.3	Numerical simulations for delayed PD controlled skateboard for the statically unstable case at low speed . . . . .	70
E.4	Numerical simulations for delayed PD controlled skateboard for the dynamically unstable case . . . . .	71

---

# List of Tables

2.1	Parameters of the skater and the board . . . . .	13
2.2	Structure of phase-space . . . . .	21
3.1	Number of positive solutions for $\tilde{\omega}^2$ . . . . .	39
3.2	Parameters for the stability charts . . . . .	44
A.1	Values of parameters and initial conditions for totally self-balancing skateboard in the stable case . . . . .	50
A.2	Values of parameters and initial conditions for totally self-balancing skateboard in dynamically unstable case . . . . .	51
A.3	Values of parameters and initial conditions for totally self-balancing skateboard in the statically unstable case . . . . .	52
A.4	Values of parameters and initial conditions for the totally self-balancing skateboard with large perturbation . . . . .	53
C.1	Values of parameters and initial conditions for nearly self-balancing skateboard in the stable case . . . . .	57
C.2	Values of parameters and initial conditions for nearly self-balancing skateboard in the dynamically unstable case . . . . .	58
C.3	Values of parameters and initial conditions for nearly self-balancing skateboard in the statically unstable case . . . . .	59
C.4	Values of parameters and initial conditions for nearly self-balancing skateboard with big perturbation . . . . .	60
D.1	Values of parameters and initial conditions for PD controlled skateboard in the stable case with $P$ less than $P_c$ and negative $a$ . . . . .	62
D.2	Values of parameters and initial conditions for PD controlled skateboard in the stable case with $P$ less than $P_c$ and positive $a$ . . . . .	63
D.3	Values of parameters and initial conditions for PD controlled skateboard in the stable case with $P$ more than $P_c$ . . . . .	64

---

D.4	Values of parameters and initial conditions for PD controlled skateboard in the unstable case with $P$ less than $P_c$ . . . . .	65
D.5	Values of parameters and initial conditions for PD controlled skateboard in the unstable case with $P$ more than $P_c$ . . . . .	66
E.1	Values of parameters and initial conditions for delayed PD controlled skateboard for the stable case . . . . .	68
E.2	Values of parameters and initial conditions for delayed PD controlled skateboard for the statically unstable case . . . . .	69
E.3	Values of parameters and initial conditions for delayed PD controlled skateboard for the statically unstable case at low speed . . . . .	70
E.4	Values of parameters and initial conditions for delayed PD controlled skateboard for the dynamically unstable case . . . . .	71

# Chapter 1

## Introduction

The simplest vehicles, even those which have been invented many years ago, sometimes show interesting instabilities. For example, the stability of bicycles (Koolijman *et al.*, 2011) (Wisse and Schwab, 2005) and skateboards (Kremnev and Kuleshov, 2008) is investigated even nowadays in several studies of vehicle dynamics. Lots of interesting videos can be found on the internet on video sharing sites (YouTube, 2013b,c,d,a). These show that it is difficult to hold the straight motion of a skateboard over a certain speed.

The first skateboard was made by the Americans in the sixties, when young Californian people installed wheels on their surfboard. Thus getting down to the seaside was became easier and faster (Szabadban.hu, 2013). In the seventies, the first skateboard production companies were founded and as far back as 1979 the first mechanical model was constructed by M. Hubbard (Hubbard, 1979, 1980). His motivation to write his study was the riders' serious injuries. This is surprising to people, who live in the Middle of Europe, for example to Hungarian people, because there the skateboard was only introduced in the late eighties. It became more popular in the new millennium.

Nowadays the skateboard is used as means of transport and doing tricks. If the speed is enough high, as the videos are shown, the riding can be dangerous, it depends on the board, the rider and the speed.

The aim of this study is to construct a useful and simple mechanical model, which helps to understand this instability in linear and nonlinear cases.

# Chapter 2

## The self-balancing skateboard

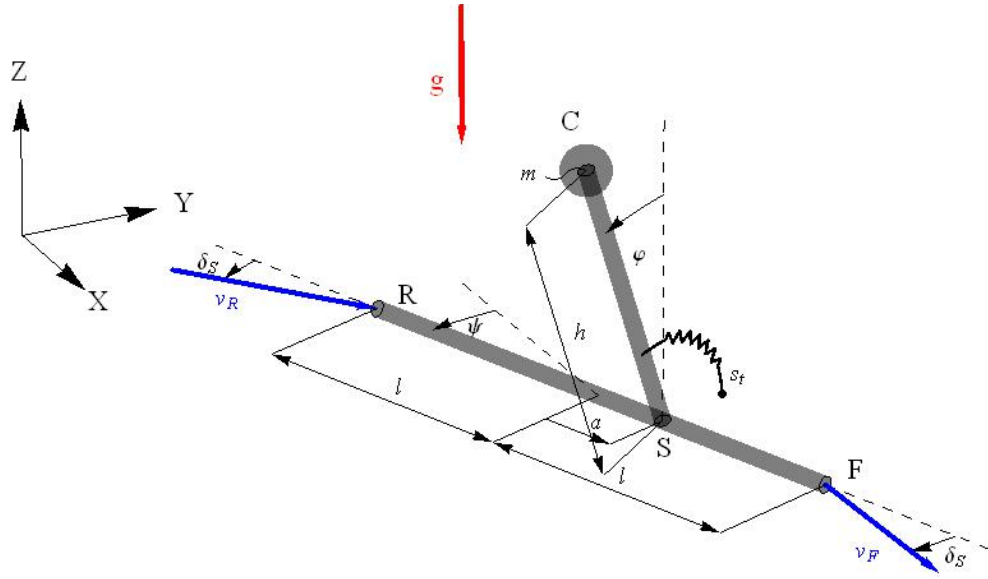
In this chapter two mechanical models are used to investigate the behaviour of the skateboard's motion. The first model consists of two kinematic constraints, the second one three. Both models consist of one mass point and two massless rods, together with one torsion spring. The equations of motion are derived with the help of the Appell-Gibbs equations (Gantmacher, 1975). After the construction of the equations' the models' linear stability is investigated. The nonlinear behaviour of the system is also analysed. These two models will be compared in this chapter.

### 2.1 Self-balancing skateboard

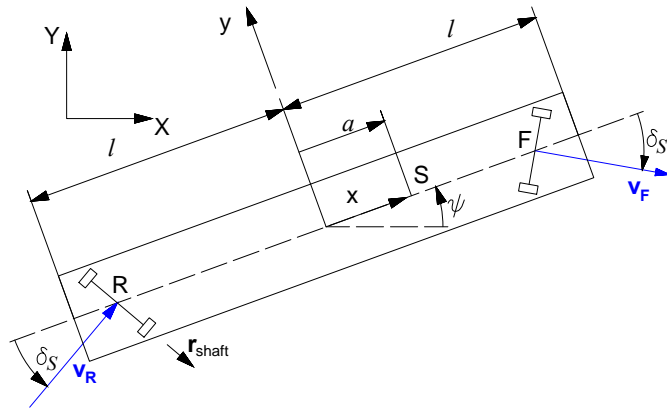
In this section the self-balancing skateboard model is derived, in the absence of human control.

#### 2.1.1 Mechanical model

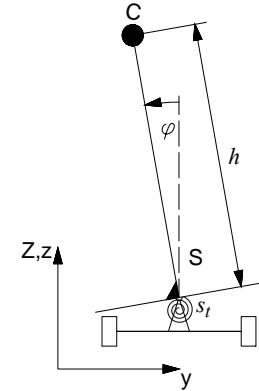
This mechanical model consists of one mass point (C) and two massless rods (RF and CS), see in Figure 2.1. The model has 6 degrees of freedom. The board must always be in contact with the ground. This reduces the number of degrees of freedom by 2. Therefore 4 generalised coordinates are required:  $X$  and  $Y$  are the coordinates of the point S,  $\psi$  is the direction of the skateboard longitudinal axis and  $\varphi$  is the tilt of the board. The model parameters are:  $h$ , the half height of the skater,  $l$  the half length of the board,  $a$  the eccentricity of the skater on the board,  $m$ , the mass point representing the mass of the skater and  $s_t$  represents the strength of the rubber element of the suspension. The



(a) The mechanical model



(b) Explanation from top view



(c) Explanation from front view

**Figure 2.1:** Mechanical model of the self-balancing skateboard

generalised coordinates and other parameters are shown in Figure 2.1. We write

$$\mathbf{q}(t) = \begin{bmatrix} X(t) \\ Y(t) \\ \psi(t) \\ \varphi(t) \end{bmatrix}, \quad \dot{\mathbf{q}}(t) = \frac{d\mathbf{q}(t)}{dt} = \begin{bmatrix} \dot{X}(t) \\ \dot{Y}(t) \\ \dot{\psi}(t) \\ \dot{\varphi}(t) \end{bmatrix} \quad \text{and} \quad \ddot{\mathbf{q}}(t) = \frac{d^2\mathbf{q}(t)}{dt^2} = \begin{bmatrix} \ddot{X}(t) \\ \ddot{Y}(t) \\ \ddot{\psi}(t) \\ \ddot{\varphi}(t) \end{bmatrix}. \quad (2.1.1)$$

The two kinematic constraints correspond to the fact that velocity direction at F (front)

and  $R$  (rear) depend on  $\varphi$  through the suspension geometry, as shown in Figure 2.2. This connection is going to be determined in the coordinate system  $(x, y, z)$  relative to the board.

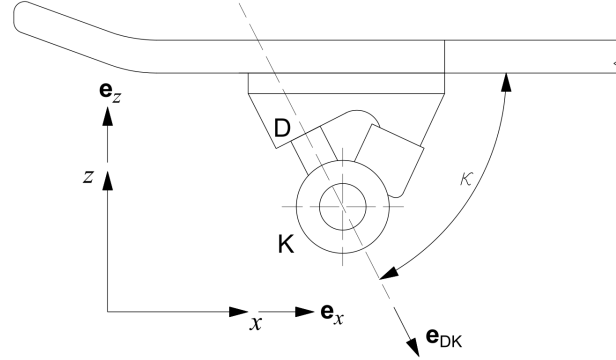


**Figure 2.2:** Suspension geometry

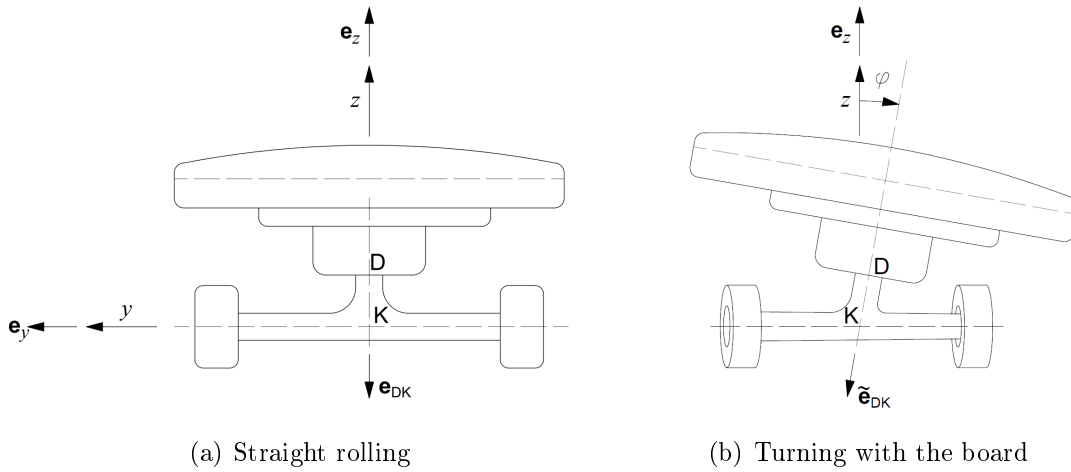


**Figure 2.3:** Turning mechanism of skateboard

When the board is tilted through an angle  $\varphi$  around the axis  $x$  the unit vector  $\mathbf{e}_{DK}$  is turned through the same angle (see in Figure 2.3(b)):

$$\tilde{\mathbf{e}}_{DK} = \mathbf{R} \cdot \mathbf{e}_{DK}, \quad (2.1.2)$$

where  $\mathbf{R}$  is a rotation matrix

$$\mathbf{R} = \begin{bmatrix} 1 & 0 & 0 \\ 0 & \cos \varphi & -\sin \varphi \\ 0 & \sin \varphi & \cos \varphi \end{bmatrix} \text{ and } \mathbf{e}_{DK} = \begin{bmatrix} \cos \kappa \\ 0 \\ -\sin \kappa \end{bmatrix}. \quad (2.1.3)$$

The wheel shaft and the shaft DK are connected rigidly, this is one element of the suspension. So they must be perpendicular for an  $\varphi$  values, thus the wheel shaft vector  $\mathbf{r}_{\text{shaft}}$  (see in Figure 2.1(b)), which connects the two wheels, must be perpendicular with  $\tilde{\mathbf{e}}_{\text{DK}}$ . Moreover it is parallel with the ground, so the wheel shaft and axes  $z$  (the unit vector in this direction is  $\mathbf{e}_z$ ) are perpendicular. On this basis:

$$\mathbf{r}_{\text{shaft}} = \tilde{\mathbf{e}}_{\text{DK}} \times \mathbf{e}_z. \quad (2.1.4)$$

The angle between the velocity of the wheels' centre and the  $x$  axis is the same as the angle between the shaft and axes  $y$ . This is the steering angle  $\delta_S$ . The cosine of the steering angle is determined by the scalar product:

$$\mathbf{r}_{\text{shaft}} \cdot \mathbf{e}_y = |\mathbf{r}_{\text{shaft}}| \cos \delta_S. \quad (2.1.5)$$

The connection between angle  $\varphi$  and angle  $\delta$  is obtained from equation (2.1.5):

$$\sin \varphi \tan \kappa = \tan \delta_S. \quad (2.1.6)$$

## 2.1.2 Skater's state of motion

In this subsection the velocity and the acceleration of the point C will be defined. The calculations are performed in the coordinate system  $(X, Y, Z)$  fixed to the ground. The velocity of point S is

$$\mathbf{v}_S = \begin{bmatrix} \dot{X} & \dot{Y} & 0 \end{bmatrix}^T \quad (2.1.7)$$

and the angular velocity of the rigid body is

$$\boldsymbol{\omega} = \begin{bmatrix} \dot{\varphi} \cos \psi & \dot{\varphi} \sin \psi & \dot{\psi} \end{bmatrix}^T. \quad (2.1.8)$$

The velocity of point C,  $\mathbf{v}_C$  is determined with the help of rigid body kinematics:

$$\mathbf{v}_C = \mathbf{v}_S + \boldsymbol{\omega} \times \mathbf{r}_{\text{SC}}, \quad (2.1.9)$$

where  $\mathbf{r}_{\text{SC}}$  is the vector from S to C given by

$$\mathbf{r}_{\text{SC}} = \begin{bmatrix} h \sin \varphi \sin \psi & -h \sin \varphi \cos \psi & h \cos \varphi \end{bmatrix}^T. \quad (2.1.10)$$

From the (2.1.9) and (2.1.10) we find that

$$\mathbf{v}_C = \begin{bmatrix} \dot{X} + h\dot{\varphi} \cos \varphi \sin \psi + h\dot{\psi} \sin \varphi \cos \psi \\ \dot{Y} - h\dot{\varphi} \cos \varphi \cos \psi + h\dot{\psi} \sin \varphi \sin \psi \\ -h\dot{\varphi} \sin \varphi \end{bmatrix} \quad (2.1.11)$$

and the same velocity in a local coordinate system is given by:

$$\mathbf{v}_{C_{CR3}} = \begin{bmatrix} \cos \psi \dot{X} + \sin \psi \dot{Y} + h \sin \varphi \dot{\psi} \\ -\cos \varphi \sin \psi \dot{X} + \cos \varphi \cos \psi \dot{Y} - h \dot{\varphi} \\ \sin \varphi \sin \psi \dot{X} - \sin \varphi \cos \psi \dot{Y} \end{bmatrix}. \quad (2.1.12)$$

The acceleration of the point C,  $\mathbf{a}_C$  is computed in the same way:

$$\mathbf{a}_C = \mathbf{a}_S + \boldsymbol{\varepsilon} \times \mathbf{r}_{SC} + \boldsymbol{\omega} \times (\boldsymbol{\omega} \times \mathbf{r}_{SC}), \quad (2.1.13)$$

where

$$\mathbf{a}_S = \dot{\mathbf{v}}_S, \quad \boldsymbol{\varepsilon} = \dot{\boldsymbol{\omega}} = \begin{bmatrix} -\dot{\varphi}\dot{\psi} \sin \psi + \ddot{\varphi} \cos \psi \\ \dot{\varphi}\dot{\psi} \cos \psi + \ddot{\varphi} \sin \psi \\ \ddot{\psi} \end{bmatrix}. \quad (2.1.14)$$

Evaluating we find that:

$$\mathbf{a}_C = \begin{bmatrix} \ddot{X} + h \sin \psi \left( \ddot{\varphi} \cos \varphi - (\dot{\varphi}^2 + \dot{\psi}^2) \sin \varphi \right) + h \cos \psi \left( 2\dot{\varphi}\dot{\psi} \cos \varphi + \ddot{\psi} \sin \varphi \right) \\ \ddot{Y} + h \sin \varphi \left( \ddot{\psi} \sin \psi + (\dot{\varphi}^2 + \dot{\psi}^2) \cos \psi \right) + h \cos \varphi \left( 2\dot{\varphi}\dot{\psi} \sin \psi + \ddot{\psi} \cos \psi \right) \\ -h (\dot{\varphi}^2 \cos \varphi + \ddot{\varphi} \sin \varphi) \end{bmatrix}. \quad (2.1.15)$$

### 2.1.3 Kinematic constraints

The velocities  $\mathbf{v}_F$ ,  $\mathbf{v}_R$  of points F, R are determined by  $\mathbf{v}_S$  and  $\boldsymbol{\omega}$ , as well as the directions of the velocity of these points (see Figure 2.1).

Hence

$$\mathbf{v}_F = \mathbf{v}_S + \boldsymbol{\omega} \times \mathbf{r}_{SF}, \quad (2.1.16)$$

where  $\mathbf{r}_{SF}$  is the vector from S to F, and the velocity  $\mathbf{v}_F$  is known from the kinematic constraint (see Figure 2.1):

$$\mathbf{v}_F = \begin{bmatrix} v_F \cos(\psi - \delta) & v_F \sin(\psi - \delta) & 0 \end{bmatrix}^T, \quad (2.1.17)$$

where  $v_F = \mathbf{v}_F$ .

The two equations for  $\mathbf{v}_F$  (2.1.16) and (2.1.17) must be equal. This system consist three scalar equations, one in the direction of  $X$ , one in  $Y$  and on in  $Z$ . The third equation, it is trivial. The magnitude of  $\mathbf{v}_F$  is irrelevant, so it can be eliminated from the equations. Thus the connection between the generalised coordinates and velocities is found. This is the equation of the first kinematic constraint:

$$(-\sin \psi + \cos \psi \sin \varphi \tan \kappa) \dot{X} + (\cos \psi + \sin \psi \sin \varphi \tan \kappa) \dot{Y} + (-a + l) \dot{\psi} = 0. \quad (2.1.18)$$

The kinematic constraint about the velocity  $\mathbf{v}_R$  of the point R is derived in the same way to obtain:

$$(\sin \psi + \cos \psi \sin \varphi \tan \kappa) \dot{X} + (-\cos \psi + \sin \psi \sin \varphi \tan \kappa) \dot{Y} + (a + l) \dot{\psi} = 0. \quad (2.1.19)$$

The kinematic constraints (2.1.18) and (2.1.19) can be written in matrix form:

$$\mathbf{A}\dot{\mathbf{q}} + \mathbf{A}_0 = \mathbf{0}, \quad (2.1.20)$$

where

$$\mathbf{A} = \begin{bmatrix} -\sin \psi + \cos \psi \sin \varphi \tan \kappa & \cos \psi + \sin \psi \sin \varphi \tan \kappa & -a + l & 0 \\ \sin \psi + \cos \psi \sin \varphi \tan \kappa & -\cos \psi + \sin \psi \sin \varphi \tan \kappa & a + l & 0 \end{bmatrix} \quad (2.1.21)$$

and

$$\mathbf{A}_0 = \begin{bmatrix} 0 & 0 \end{bmatrix}^T. \quad (2.1.22)$$

#### 2.1.4 Equation of motion

The equations of motion of this non-holonomic system can be derived with the help of Appell-Gibbs equations (Gantmacher, 1975). In this method, pseudo velocities must be chosen. The pseudo velocities are produced as the linear combination of generalised velocities, like the kinematic constraints in (2.1.20). The pseudo velocities can be chosen intuitively, but they must describe the system uniquely. In our case two pseudo velocities are required, the first one can be taken to be the longitudinal velocity of the point S, and the second one could be the angular velocity of the skater according to the board:

$$\rho := \dot{X} \cos \psi + \dot{Y} \sin \psi, \quad (2.1.23a)$$

$$\sigma := \dot{\psi}. \quad (2.1.23b)$$

The kinematic constraints and the definitions of the pseudo velocities can be written in matrix form:

$$\begin{bmatrix} \mathbf{A} \\ \mathbf{B} \end{bmatrix} \dot{\mathbf{q}} = \begin{bmatrix} -\mathbf{A}_0 \\ \boldsymbol{\sigma} \end{bmatrix}, \quad (2.1.24)$$

where the vector of the pseudo velocities is denoted by  $\boldsymbol{\sigma}$  and the  $\mathbf{B}$  matrix represents the definition of the pseudo velocities (2.1.23):

$$\boldsymbol{\sigma} = \begin{bmatrix} \rho \\ \sigma \end{bmatrix}. \quad \text{and} \quad \mathbf{B} = \begin{bmatrix} \cos \psi & \sin \psi & 0 & 0 \\ 0 & 0 & 0 & 1 \end{bmatrix} \quad (2.1.25)$$

The solution of equation (2.1.24) gives the generalised velocities in terms of the generalised coordinates and the pseudo velocities:

$$\begin{bmatrix} \dot{X} \\ \dot{Y} \\ \dot{\psi} \\ \dot{\varphi} \end{bmatrix} = \begin{bmatrix} (\cos \psi + \frac{a}{l} \sin \varphi \sin \psi \tan \kappa) \rho \\ (\sin \psi - \frac{a}{l} \sin \varphi \cos \psi \tan \kappa) \rho \\ -\sin \varphi \frac{\tan \kappa}{l} \rho \\ \sigma \end{bmatrix}, \quad (2.1.26)$$

The generalised accelerations are determined by deriving both sides of equation (2.1.26) with respect to time

$$\begin{bmatrix} \ddot{X} \\ \ddot{Y} \\ \ddot{\psi} \\ \ddot{\varphi} \end{bmatrix} = \begin{bmatrix} \tan \kappa \left( \sin \varphi \dot{Y} + a \cos \varphi \sin \varphi \sigma \right) \rho + \dot{X} \frac{\dot{\rho}}{\rho} \\ -\tan \kappa \left( \sin \varphi \dot{X} + a \cos \varphi \cos \psi \sigma \right) \rho + \dot{Y} \frac{\dot{\rho}}{\rho} \\ -\tan \kappa (\cos \varphi \rho \sigma + \sin \varphi \dot{\rho}) \\ \dot{\sigma} \end{bmatrix}. \quad (2.1.27)$$

$\mathcal{A}$  denotes the *energy of acceleration* used in the construction of the Appell-Gibbs equations:

$$\frac{\partial \mathcal{A}}{\partial \dot{\rho}} = \Omega, \quad (2.1.28a)$$

$$\frac{\partial \mathcal{A}}{\partial \dot{\sigma}} = \Gamma, \quad (2.1.28b)$$

where  $\Omega$  and  $\Gamma$  the so-called *pseudo forces*. The pseudo forces can be derived from the virtual power of the active forces generated by the spring and gravity. The virtual power is given by

$$\delta P = \mathbf{G} \cdot \delta \mathbf{v}_C + \mathbf{M}_{st} \cdot \delta \boldsymbol{\omega} = \Omega \delta \rho + \Gamma \delta \sigma, \quad (2.1.29)$$

where

$$\mathbf{G} = \begin{bmatrix} 0 & 0 & -mg \end{bmatrix}^T \quad \text{and} \quad \mathbf{M}_{s_t} = \begin{bmatrix} -s_t \sinh \varphi \cos \psi & -s_t \sinh \varphi \sin \psi & 0 \end{bmatrix}^T \quad (2.1.30)$$

and  $\delta$  denotes virtual quantities. The pseudo forces  $\Omega$  and  $\Gamma$  are found from equation (2.1.29):

$$\Omega = 0 \quad \text{and} \quad \Gamma = mgh \sin \varphi - s_t \sinh \varphi. \quad (2.1.31)$$

With the known pseudo forces, only the energy of acceleration is missing for the Appell-Gibbs equations. The energy of acceleration is computed easily when the model consists of only one mass point:

$$\mathcal{A} = \frac{1}{2} m \mathbf{a}_C \cdot \mathbf{a}_C. \quad (2.1.32)$$

In this case the energy of acceleration is given by:

$$\begin{aligned} \mathcal{A} = & -(\rho \cos \varphi (\tan \kappa (-2a^2 + 3h^2 \cos(2\varphi) - 3h^2) + 6hl) + 2ahl\sigma \sin \varphi) \cdot \\ & \cdot \frac{m}{2l^2} \tan \kappa \sigma \sin \varphi \dot{\rho} + \frac{a}{l} hm \tan \kappa \sin \varphi \cos \varphi \dot{\rho} \dot{\sigma} + \frac{mh^2}{2} \dot{\sigma}^2 + \\ & + \frac{mh}{l^2} \tan \kappa \rho \cos \varphi (a\sigma \cos \varphi + \rho \sin \varphi (l - h \tan \kappa \sin^2 \varphi)) \dot{\sigma} + \\ & + \frac{m}{2l^2} (\tan \kappa \sin^2 \varphi (\tan \kappa (a^2 + h^2 \sin^2 \varphi) - 2hl) + l^2) \dot{\rho}^2 + \dots \end{aligned} \quad (2.1.33)$$

The energy of acceleration and the pseudo forces can be written in the form

$$\begin{aligned} \frac{\mathcal{A}}{mh^2} = & \left( \frac{1}{2} (3\theta_h^2 \sin^2 \varphi - 3\theta_h + \theta_a^2) \tilde{\rho} \sin(2\varphi) - \theta_a \sigma \sin^2 \varphi \right) \sigma \dot{\tilde{\rho}} + \\ & + \left( \frac{1}{2} \theta_h (1 - \theta_h \sin^2 \varphi) \tilde{\rho} \sin(2\varphi) + \theta_a (1 - \sin^2 \varphi) \sigma \right) \tilde{\rho} \dot{\sigma} + \\ & + \frac{1}{2} \theta_a \sin(2\varphi) \tilde{\rho} \dot{\sigma} + \left( (\theta_h \sin^2 \varphi - 1)^2 + \theta_a^2 \sin^2 \varphi \right) \frac{1}{2} \tilde{\rho}^2 + \frac{1}{2} \dot{\sigma}^2 + \dots, \end{aligned} \quad (2.1.34a)$$

$$\frac{\Omega}{mh^2} = 0 \quad \text{and} \quad \frac{\Gamma}{mh^2} = \alpha_g^2 \sin \varphi - \alpha_{s_t}^2 \sinh \varphi, \quad (2.1.34b)$$

where the new parameters are given by:

$$\tilde{\rho} := \frac{\rho}{h}, \quad \theta_a := \frac{a}{l} \tan \kappa, \quad \theta_h := \frac{h}{l} \tan \kappa, \quad \alpha_g^2 := \frac{g}{h} \quad \text{and} \quad \alpha_{s_t}^2 := \frac{s_t}{mh^2}. \quad (2.1.35)$$

From now on  $\tilde{\rho}$  is used as a pseudo velocity instead of  $\rho$ . This  $\tilde{\rho}$  can be called the *relative longitudinal velocity*.

Then the equations of motion can be calculated with the help of Appell-Gibbs equations:

$$\dot{\tilde{\rho}} = \frac{A_\rho(\varphi, \sigma, \tilde{\rho})}{B(\varphi)}, \quad (2.1.36a)$$

$$\dot{\sigma} = C(\varphi, \sigma, \tilde{\rho}) + \frac{A_\sigma(\varphi, \sigma, \tilde{\rho})}{B(\varphi)}, \quad (2.1.36b)$$

where

$$A_\rho(\varphi, \sigma, \tilde{\rho}) = \frac{1}{2}\theta_a \sin(2\varphi) (\alpha_{st}^2 \sinh \varphi - \alpha_g^2 \sin \varphi) - \frac{1}{4}\theta_a \theta_h (\theta_h \sin^2 \varphi - 1) \tilde{\rho}^2 \sin^2(2\varphi) + \frac{1}{2} (3\theta_h (1 - \theta_h \sin \varphi) - \theta_a^2 \sin^2 \varphi) \tilde{\rho} \sigma \sin(2\varphi) + \theta_a \sigma^2 \sin^2 \varphi, \quad (2.1.37a)$$

$$B(\varphi) = \theta_a^2 \sin^4 \varphi + (\theta_h \sin^2 \varphi - 1)^2, \quad (2.1.37b)$$

$$C(\varphi, \sigma, \tilde{\rho}) = \frac{1}{2}\theta_h \sin(2\varphi) (\theta_h \sin^2 \varphi - 1) \tilde{\rho}^2 + \theta_a (\sin^2 \varphi - 1) \tilde{\rho} \sigma + \alpha_g^2 \sin \varphi - \alpha_{st}^2 \sinh \varphi \quad (2.1.37c)$$

$$A_\sigma(\varphi, \sigma, \tilde{\rho}) = -\frac{1}{2}\theta_a \sin^2 \varphi A_\rho(\varphi, \sigma, \tilde{\rho}) \quad (2.1.37d)$$

are functions of the two pseudo velocities  $\tilde{\rho}$  and  $\sigma$  and the generalised coordinate  $\varphi$ . Note that these expressions are independent of the other three generalised coordinates  $X$ ,  $Y$  and  $\psi$ .

The skateboard's equations of the motion are obtained from the Appell-Gibbs equations (2.1.36) and from the formula of the general velocities (2.1.26):

$$\dot{\tilde{\rho}} = \frac{A_\rho(\varphi, \sigma, \tilde{\rho})}{B(\varphi)}, \quad (2.1.38a)$$

$$\dot{\sigma} = C(\varphi, \sigma, \tilde{\rho}) + \frac{A_\sigma(\varphi, \sigma, \tilde{\rho})}{B(\varphi)}, \quad (2.1.38b)$$

$$\dot{\varphi} = \sigma, \quad (2.1.38c)$$

$$\frac{\dot{X}}{h} = (\cos \psi + \theta_a \sin \varphi \sin \psi) \tilde{\rho}, \quad (2.1.38d)$$

$$\frac{\dot{Y}}{h} = (\sin \psi - \theta_a \sin \varphi \cos \psi) \tilde{\rho}, \quad (2.1.38e)$$

$$\dot{\psi} = -\theta_h \sin \varphi \tilde{\rho}, \quad (2.1.38f)$$

The first three equations of (2.1.38) are independent of  $X$ ,  $Y$  and  $\psi$ , so they can be decoupled from the last three. This means that  $X$ ,  $Y$  and  $\psi$  are cyclic coordinates and the first three equations (2.1.38a), (2.1.38b) and (2.1.38c) describe the system uniquely in the three dimensional phase space of the relative longitudinal velocity  $\tilde{\rho}$ , the angular velocity of

the skater  $\sigma$  and the tilt of the skater  $\varphi$ .

From now on, the straight stationary motion of the skateboard with  $V$  longitudinal velocity is investigated. The values of the state variables during this motion are the following:

$$\tilde{\rho} = V/h =: \alpha_V, \quad (\rho = V), \quad \sigma = 0, \quad \varphi = 0, \quad X = Vt, \quad Y = 0 \quad \text{and} \quad \psi = 0. \quad (2.1.39)$$

### 2.1.5 Linear stability analysis of the straight line motion

To investigate the stability of straight line motion, only the first three equations from the equation of motion (2.1.38) are used, as was mentioned before. The linear equations of motion around the stationary solution with the respect to small perturbations  $\tilde{\rho}$ ,  $\sigma$  and  $\varphi$  are shown in the form:

$$\dot{\mathbf{X}} = \mathbf{J}(\mathbf{X} - \mathbf{X}_0), \quad (2.1.40)$$

where

$$\mathbf{X} = \begin{bmatrix} \tilde{\rho} \\ \sigma \\ \varphi \end{bmatrix}, \quad \mathbf{X}_0 = \begin{bmatrix} \alpha_V \\ 0 \\ 0 \end{bmatrix} \quad \text{and} \quad \mathbf{J} = \begin{bmatrix} 0 & 0 & 0 \\ 0 & -\alpha_V\theta_a & \alpha_g^2 - \alpha_{s_t}^2 - \alpha_V^2\theta_h \\ 0 & 1 & 0 \end{bmatrix}. \quad (2.1.41)$$

It can be seen, that the motion is independent of the relative longitudinal velocity  $\tilde{\rho}$ .

For the stability analysis of linear ordinary differential equations, the *Routh-Hurwitz stability criteria* can be used (Gantmacher, 1975).

The characteristic equation of this differential equation system is

$$\det(\lambda\mathbf{I} - \mathbf{J}) = 0, \quad (2.1.42)$$

which can be written as

$$\lambda^3 + \alpha_V\theta_a\lambda^2 + (-\alpha_g^2 + \alpha_{s_t}^2 + \alpha_V^2\theta_h)\lambda = 0. \quad (2.1.43)$$

The Hurwitz determinant  $H_i$  can be derived from the coefficients of the characteristic

polynomial:

$$H_1 = \alpha_V \theta_a, \quad (2.1.44a)$$

$$H_2 = \begin{vmatrix} \alpha_V \theta_a & 0 \\ 1 & -\alpha_g^2 + \alpha_{s_t}^2 + \alpha_V^2 \theta_h \end{vmatrix}, \quad (2.1.44b)$$

$$H_3 = \begin{vmatrix} \alpha_V \theta_a & 0 & 0 \\ 1 & -\alpha_g^2 + \alpha_{s_t}^2 + \alpha_V^2 \theta_h & 0 \\ 0 & \alpha_V \theta_a & 0 \end{vmatrix}. \quad (2.1.44c)$$

As known from the Routh-Hurwitz condition: for all roots of the characteristic equation to have negative real part, it is necessary and sufficient that all  $H_i$  are positive. The conditions in our case are

$$\alpha_V \theta_a > 0, \quad (2.1.45a)$$

$$-\alpha_g^2 + \alpha_{s_t}^2 + \alpha_V^2 \theta_h > 0, \quad (2.1.45b)$$

$$0 > 0. \quad (2.1.45c)$$

Parameter  $m$ ,  $h$ ,  $l$  and  $\tan \kappa$  can be assumed to be positive. The three criteria with the original parameters are as follows:

$$aV > 0, \quad (2.1.46a)$$

$$s_t - mgh + mV^2 \frac{h}{l} \tan \kappa > 0, \quad (2.1.46b)$$

$$0 > 0. \quad (2.1.46c)$$

From (2.1.46c) it can be seen easily, that this equilibrium can not be stable at any parameter values. This is obvious, because the characteristic equation (2.1.43) has got one zero root, thus the third Hurwitz determinant ( $H_3$ ) is zero. The lack of connection between  $\rho$  and the another variables in the linear case causes the zero root. In the linear case  $\rho$  is also a cyclic coordinate. If we dispense with  $\rho$ , the equilibrium is asymptotic stable, else it is stable only in *Lyapunov* case.

In the following a few explanations are given for the physical understanding of criteria (2.1.46). The first means the skater has to stand in front of the centre of the skateboard. This is not unusual, the skiers do the same, they lean forward. The second one means the torsion spring has to be stiff enough. It is also seen, that the longitudinal velocity ( $V$ ) helps to stabilize the motion. The same happens with the bicycles (Koolijman *et al.*, 2011).

Based on the stability criteria (2.1.46), a stability chart can be created, see in Figure 2.4.

In this figure the required spring stiffness ( $s_t$ ) is plotted as function of longitudinal velocity ( $V$ ). The stable domain is coloured by grey, the unstable one is coloured by white. To draw Figure 2.4, we have used realistic parameter values, as given in Table 2.1.

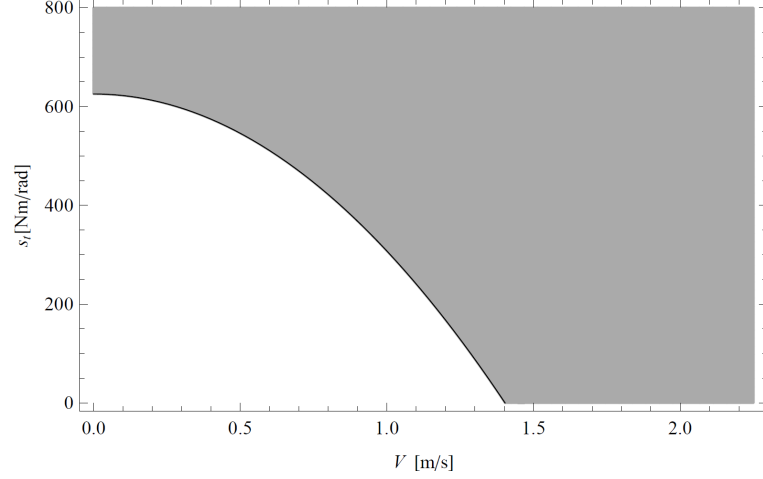


**Figure 2.4:** Stability chart of the totally self-balancing skateboard

**Table 2.1:** Parameters of the skater and the board

$h$	$m$	$g$	$l$	$\kappa$
[m]	[kg]	[ms <sup>-2</sup> ]	[m]	[°]
0.85	75	9.81	0.3937	63

From the (2.1.46b) stability criterion, the critical spring stiffness ( $s_{t,c}$ ) and longitudinal velocity ( $V_c$ ) are given by:

$$s_{t,c} = mgh - mV^2 \frac{h}{l} \tan \kappa, \quad \alpha_{s_{t,c}}^2 = \alpha_g^2 - \alpha_V^2 \theta_h, \quad (2.1.47a)$$

$$V_c = \sqrt{g - \frac{s_t}{mh}} \sqrt{\frac{l}{\tan \kappa}}, \quad \alpha_{V,c}^2 = \frac{\alpha_g^2 - \alpha_{s_t}^2}{\theta_h}. \quad (2.1.47b)$$

We can get the same stability chart for negative  $V$ .

## 2.1.6 Nonlinear Analysis

The aim of this section is to discover the behaviour of the motion in the nonlinear domain, creating a bifurcation diagram. First other equilibria will be found, then the existence of limit cycles will be studied.

To investigate equilibria the first three equations (2.1.38a), (2.1.38b) and (2.1.38c) are

used. The derivatives must be zero to be an equilibrium, so from the third equation

$$\sigma = 0, \quad (2.1.48)$$

this is put to use in the first two ones, we find:

$$0 = \frac{\theta_a \sin(2\varphi)}{(\theta_h \sin^2 \varphi - 1)^2 + \theta_a^2 \sin^4 \varphi} E(\varphi, \tilde{\rho}), \quad (2.1.49a)$$

$$0 = \frac{(\theta_h \sin^2 \varphi - 1)^2 + \theta_a^2 \sin^2 \varphi}{(\theta_h \sin^2 \varphi - 1)^2 + \theta_a^2 \sin^4 \varphi} E(\varphi, \tilde{\rho}), \quad (2.1.49b)$$

where

$$E(\varphi, \tilde{\rho}) = \alpha_{st}^2 \sinh \varphi - \alpha_g^2 \sin \varphi + \frac{1}{2} \theta_h \sin(2\varphi) (\theta_h \sin^2 \varphi - 1) \tilde{\rho}^2. \quad (2.1.50)$$

Hence to investigate equilibria, it is sufficient to examine the zeros of  $E(\varphi, \tilde{\rho})$  is sufficient hereafter.

Henceforward the  $\alpha_V$  variable is used instead of  $\tilde{\rho}$  since  $V/h = \alpha_V$  denotes the investigated equilibrium of  $\tilde{\rho}$ . With this change equations (2.1.49) are given in the new form:

$$\alpha_{st}^2 \sinh \varphi = \alpha_g^2 \sin \varphi + \frac{1}{2} \alpha_V^2 \theta_h \sin(2\varphi) (\theta_h \sin^2 \varphi - 1). \quad (2.1.51)$$

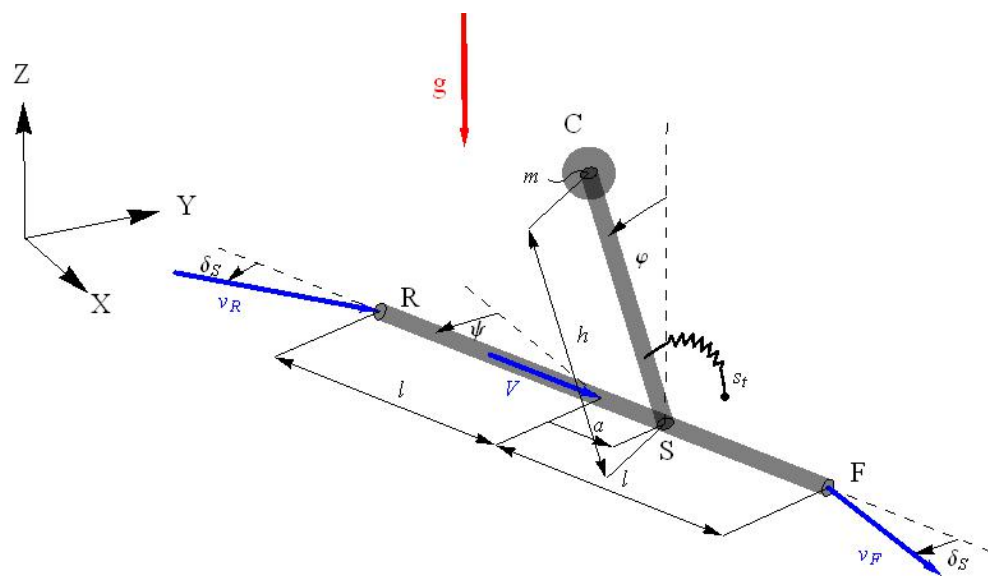
We can get the same condition while analysing *Nearly self-balancing skateboard* model, thus any further analysis of equilibria is in Section 2.2.5.

## 2.2 Nearly self-balancing skateboard

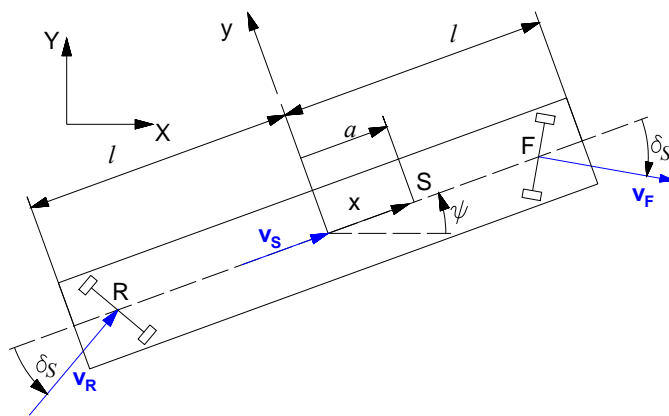
In this section the nearly self-balancing skateboard model is considered. This is very similar with the previous one, the only difference between the two models is an additional kinematic constraint. We assume that the skater keeps the longitudinal velocity of the board constant.

### 2.2.1 Mechanical model

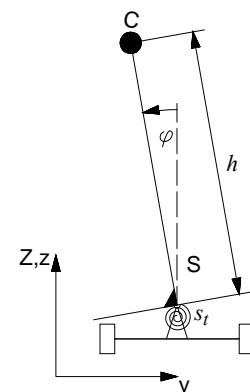
The new kinematic constraints can be seen in Figure 2.5 at point S.



(a) The mechanical model



(b) Explanation from top view



(c) Explanation from front view

**Figure 2.5:** Mechanical model of the nearly self-balancing skateboard

The magnitude of longitudinal velocity of point S must be  $V$ . Hence:

$$\dot{X} \cos \psi + \dot{Y} \sin \psi = V. \quad (2.2.1)$$

Since the other two kinematic constraints exist also, we just add another row to the matrix  $\mathbf{A}$  and vector  $\mathbf{A}_0$ :

$$\mathbf{A} = \begin{bmatrix} -\sin \psi + \cos \psi \sin \varphi \tan \kappa & \cos \psi + \sin \psi \sin \varphi \tan \kappa & -a + l & 0 \\ \sin \psi + \cos \psi \sin \varphi \tan \kappa & -\cos \psi + \sin \psi \sin \varphi \tan \kappa & a + l & 0 \\ \cos \psi & \sin \psi & 0 & 0 \end{bmatrix} \quad (2.2.2)$$

and

$$\mathbf{A}_0 = \begin{bmatrix} 0 & 0 & -V \end{bmatrix}^T. \quad (2.2.3)$$

Then the kinematic constraints can be obtained in the same way:

$$\mathbf{A}\dot{\mathbf{q}} + \mathbf{A}_0 = \mathbf{0}. \quad (2.2.4)$$

## 2.2.2 Equation of motion

The equation of motion can be constructed with the help of Appell-Gibbs equation. There is one more kinematic constraint so only one pseudo velocity is required. We take it to be the relative angular velocity of the body:

$$\sigma := \dot{\varphi}. \quad (2.2.5)$$

In this case the generalised velocities in terms of the generalised coordinates and the pseudo velocity are given by:

$$\begin{bmatrix} \dot{X} \\ \dot{Y} \\ \dot{\psi} \\ \dot{\varphi} \end{bmatrix} = \begin{bmatrix} V (\cos \psi + \frac{a}{l} \sin \varphi \sin \psi \tan \kappa) \\ V (\sin \psi - \frac{a}{l} \sin \varphi \cos \psi \tan \kappa) \\ -V \sin \varphi \frac{\tan \kappa}{l} \\ \sigma \end{bmatrix}. \quad (2.2.6)$$

The energy of acceleration can be computed the same way as (2.1.32) (the independent parts of  $\dot{\sigma}$  are niggling here too), and the result is

$$\frac{\mathcal{A}}{mh^2} = \left( \frac{1}{2} \alpha_V^2 \theta_h (1 - \theta_h \sin^2 \varphi) \sin(2\varphi) + \alpha_V \theta_a (1 - \sin^2 \varphi) \sigma \right) \dot{\sigma} + \frac{1}{2} \dot{\sigma}^2 + \dots \quad (2.2.7)$$

The pseudo force is derived similarly and the virtual power is the same, since there is

only one pseudo velocity, only one pseudo force exists, which is:

$$\frac{\Gamma}{mh^2} = \alpha_g^2 \sin \varphi - \alpha_{st}^2 \sinh \varphi. \quad (2.2.8)$$

Thus the equations of the motion are:

$$\dot{\sigma} = \alpha_g^2 \sin \varphi - \alpha_{st}^2 \sinh \varphi + \frac{1}{2} \alpha_V^2 \theta_h (\theta_h \sin^2 \varphi - 1) \sin(2\varphi) - \alpha_V \theta_a (1 - \sin^2 \varphi) \sigma, \quad (2.2.9a)$$

$$\dot{\varphi} = \sigma, \quad (2.2.9b)$$

$$\frac{\dot{X}}{h} = \alpha_V (\cos \psi + \theta_a \sin \varphi \sin \psi), \quad (2.2.9c)$$

$$\frac{\dot{Y}}{h} = \alpha_V (\sin \psi - \theta_a \sin \varphi \cos \psi), \quad (2.2.9d)$$

$$\dot{\psi} = -\alpha_V \theta_h \sin \varphi. \quad (2.2.9e)$$

The  $X$ ,  $Y$  and  $\psi$  generalised coordinates are cyclic coordinates here too, just the same as in the previous model. The investigated equilibrium is the static straight line motion, given by:

$$\sigma = 0, \quad \varphi = 0, \quad X = Vt, \quad Y = 0 \quad \text{and} \quad \psi = 0. \quad (2.2.10)$$

### 2.2.3 Conservative quantity

To check the conservative nature of the system, the Appell-Gibbs equation (2.2.9a) is used. First this equation is multiplied by  $\sigma$ , and the resulting equation is integrated with respect by time.

$$\int 0 dt = \int \sigma \dot{\sigma} dt - \int \alpha_g^2 \sin \varphi \varphi \sigma dt - \int \alpha_{st}^2 \sinh \varphi \sigma dt + \frac{1}{2} \alpha_V^2 \theta_h (1 - \theta_h \sin^2 \varphi) \sin(2\varphi) \sigma dt + \int \alpha_V \theta_a \cos^2 \varphi \sigma^2 dt. \quad (2.2.11)$$

We find

$$c_2 = \frac{1}{2} \sigma^2 + \alpha_g^2 \cos \varphi + \alpha_{st}^2 \cosh \varphi - \frac{1}{4} \alpha_V^2 \theta_h^2 \sin^4 \varphi + \frac{1}{2} \alpha_V^2 \theta_h \sin^2 \varphi + \int \alpha_V \theta_a \cos^2 \varphi \sigma^2 dt, \quad (2.2.12)$$

where  $c_2$  is a constant.

The total energy can be determined from the kinetic and potential energies:

$$E_t = E_k + E_g + E_{st}, \quad (2.2.13)$$

where

$$E_k = \alpha_V^2 + \frac{1}{2}\sigma^2 + \frac{1}{2}\theta_h^2\alpha_V^2\sin^4\varphi - \alpha_V^2\theta_h\sin^2\varphi + \frac{1}{2}\alpha_V\theta_a(\alpha_V\theta_a\sin^2\varphi + \sigma\sin(2\varphi)), \quad (2.2.14)$$

$$E_g = \alpha_g^2(\cos\varphi - 1), \quad (2.2.15)$$

$$E_{st} = \alpha_{st}^2\cosh\varphi \quad (2.2.16)$$

we find

$$E_t = \alpha_V^2 - \alpha_g^2 + \frac{1}{2}\sin^2\varphi + \alpha_g^2\cos\varphi + \alpha_{st}^2\cosh\varphi + \frac{1}{2}\theta_h^2\alpha_V^2\sin^4\varphi - \alpha_V^2\theta_h\sin^2\varphi + \frac{1}{2}\alpha_V\theta_a(\alpha_V\theta_a\sin^2\varphi + \sigma\sin(2\varphi)). \quad (2.2.17)$$

If the result (2.2.12) is compared with the total energy (2.2.17) then it can be seen that the difference between the two results is not only in the constant term. If the last term of the total energy is differentiated with respect to time, it does not give the same expression as the last term of the expression (2.2.12). Moreover the independent parts of  $\theta_a$  are not the same in the two expressions, so the total energy is not constant in time.

If  $\theta_a = 0$  then a conservative quantity does exist, given by

$$c_2 = \frac{1}{2}\sigma^2 + \alpha_g^2\cos\varphi + \alpha_{st}^2\cosh\varphi - \frac{1}{4}\alpha_V^2\theta_h^2\sin^4\varphi + \frac{1}{2}\alpha_V^2\theta_h\sin^2\varphi, \quad (2.2.18)$$

which is not the total energy. This is obvious, because the force, which keeps the velocity of the centre of the board at a constant magnitude, has a power. This force has a potential in case when  $a$  is zero, given by the difference between the computed total energy and the conservative quantity.

## 2.2.4 Linear stability analysis of the straight line motion

The linear stability analysis is carried out the same way as in the previous case. The linear system can be written in the same form as the equation (2.1.40), where

$$\mathbf{X} = \begin{bmatrix} \sigma \\ \varphi \end{bmatrix}, \quad \mathbf{X}_0 = \begin{bmatrix} 0 \\ 0 \end{bmatrix} \quad \text{and} \quad \mathbf{J} = \begin{bmatrix} -\alpha_V\theta_a & \alpha_g^2 - \alpha_{st}^2 - \alpha_V^2\theta_h \\ 1 & 0 \end{bmatrix}. \quad (2.2.19)$$

The characteristic equation is almost the same as equation (2.1.43) just expect that the zero root is missing:

$$\lambda^2 + \alpha_V\theta_a\lambda - \alpha_g^2 + \alpha_{st}^2 + \alpha_V^2\theta_h = 0, \quad (2.2.20)$$

which means the stability criteria are the same without the last one (2.1.46c):

$$\alpha_V^2 \theta_a > 0, \quad (2.2.21a)$$

$$-\alpha_g^2 + \alpha_{s_t}^2 + \alpha_V^2 \theta_h > 0. \quad (2.2.21b)$$

As a conclusion it can be said, that the two models give the same results in linear case. Thus the stability boundaries and the stability chart are the same.

## 2.2.5 Nonlinear analysis

The aim of this subsection is to show the non-linear behaviour of the model.

To investigate the equilibria the first two equations (2.2.9a) (2.2.9b) are used, as was mentioned before. We find

$$\sigma = 0, \quad (2.2.22)$$

and

$$\alpha_{s_t}^2 \sinh \varphi = \alpha_g^2 \sin \varphi + \frac{1}{2} \alpha_V^2 \theta_h \sin(2\varphi) (\theta_h \sin^2 \varphi - 1). \quad (2.2.23)$$

This equation is the same as (2.1.51), so the same result can be given on the same way (see Section 2.1.6).

For the further qualitative investigation of the equilibria we will use a specific value for  $\theta_h$ , this value is 4 (the exact value is 4.23728 with Table 2.1 data). We did this, because we can obtain a simpler analytical form. Equation 2.2.23 becomes, with this simplification:

$$\sinh \varphi = \zeta_g \sin \varphi + 2\zeta_V (\sin(2\varphi) - \sin(4\varphi)), \quad (2.2.24)$$

where  $\zeta_g$  is the ratio of the *gravitational potential energy* and the *potential energy* in the spring and  $\zeta_V$  is the ratio of the *kinetic energy* and the *potential energy*:

$$\zeta_g = \frac{\alpha_g^2}{\alpha_{s_t}^2} = \frac{mgh}{s_t}, \quad \zeta_V = \frac{\alpha_V^2}{\alpha_{s_t}^2} = \frac{mV^2}{s_t}. \quad (2.2.25)$$

In this paper we are going to investigate the  $\varphi \in [-\pi/2, \pi/2]$  domain only, because outside of it the skater will fall. The aim of this examination is to understand the structure of the phase-space diagrams in the case where  $a = 0$  (where the system is Hamiltonian and so it is conservative).

Equation (2.2.24) is solvable graphically: where the graph of the right side

$$g(\varphi) = \zeta_g \sin \varphi + 2\zeta_V (\sin(2\varphi) - \sin(4\varphi)) \quad (2.2.26)$$

crosses that of the left side

$$f(\varphi) = \sinh \varphi \quad (2.2.27)$$

One possible case can be seen in Figure 2.6, where the **red** curve is function  $f(\varphi)$  and the **blue** one is  $g(\varphi)$ .  $\varphi = 0$  always satisfies equation (2.2.24) and this is a stable equilibrium if and only if

$$1 > \zeta_g - 4\zeta_V, \quad (2.2.28)$$

which is the same stability criterion as criterion (2.2.21b) with the new parameters. Graphically this means that the tangent of the function  $f$  at  $\varphi = 0$  is greater than the tangent of function  $g$  at the same  $\varphi$ .

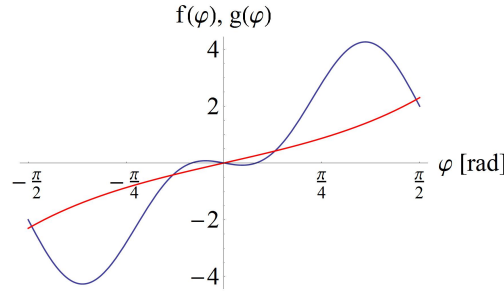


**Figure 2.6:** Graphical solution for equilibria

An other interesting point is when these two functions touches each other. It can be when the value of these functions is the same and the tangent of these functions is also the same:

$$f(\varphi) = g(\varphi) \quad \text{and} \quad \frac{df(\varphi)}{d\varphi} = \frac{dg(\varphi)}{d\varphi}. \quad (2.2.29)$$

The ratios of the energies are expressible from (2.2.29):

$$\zeta_g = \frac{\cosh(\varphi) (\sin(4\varphi) - \sin(2\varphi)) + 2 (\cos(2\varphi) - 2 \cos(4\varphi)) \sinh \varphi}{\sin^3 \varphi (6 + 12 \cos(2\varphi))}, \quad (2.2.30a)$$

$$\zeta_V = \frac{\cosh \varphi - \cot \varphi \sinh \varphi}{2 \sin^2 \varphi (6 + 12 \cos(2\varphi))}. \quad (2.2.30b)$$

And finally the structure of phase-space changes when a new equilibrium appears at the edge of the investigated domain ( $\varphi = \pi/2$ ). This happens when

$$\zeta_g = \sinh \left( \frac{\pi}{2} \right). \quad (2.2.31)$$

This three conditions (the stability of the origin (2.2.28), the condition for the connection (2.2.30) and the appearance of the equilibrium (2.2.31)) divide the space of energy ratios into five parts (see in Figure 2.7).

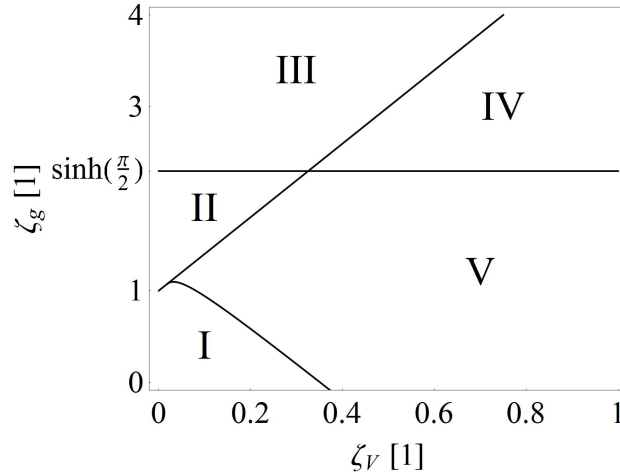


**Figure 2.7:** Different phase-space structures in the space of energy ratios

Information about the phase-space for each domain is given in Table 2.2. In the second row, there is information about the stability of the origin, *stab.* means the upper equilibrium is stable in Lyapunov case, because  $a = 0$ , *unstab.* means it is unstable, the third row of the table indicates the number of the equilibria. There is one example of every different structure in Figure 2.8.

**Table 2.2:** Structure of phase-space

Domain	I	II	III	IV	V
Stability	stab.	unstab.	unstab.	stab.	stab.
No. EP	1	3	1	3	5

As far as stability is concerned domain I is the best possibility, because there is only one stable equilibrium, which is a centre, and nothing else. Hence the stable motion of the skater remains in the case of any perturbation. Increasing the velocity (kinetic energy) we can get into domain V, where four other equilibria appear. Two saddles and two centres. The straight line motion is still stable, but this case is not as good as the previous one, because in the case of a big enough perturbation the skater is moved to the other side of the saddle, so the skater goes to a outer equilibria. This means the skater will move in a circle, but equilibria is stable, so will may fall of. The phase-space looks similar in domain IV, the difference between these two domains is that the outer equilibria move out the investigated area. In this case, there can be a stability loss at high speed if the system gets a big perturbation (for example the skater must avoid something).

If  $\zeta_g$  is increasing it means the potential energy from gravity is getting bigger than the potential energy of the spring, thus the spring is getting relatively weaker. If we start from domain I again, but we investigate the effect of increasing parameter  $\zeta_g$ , then we can reach

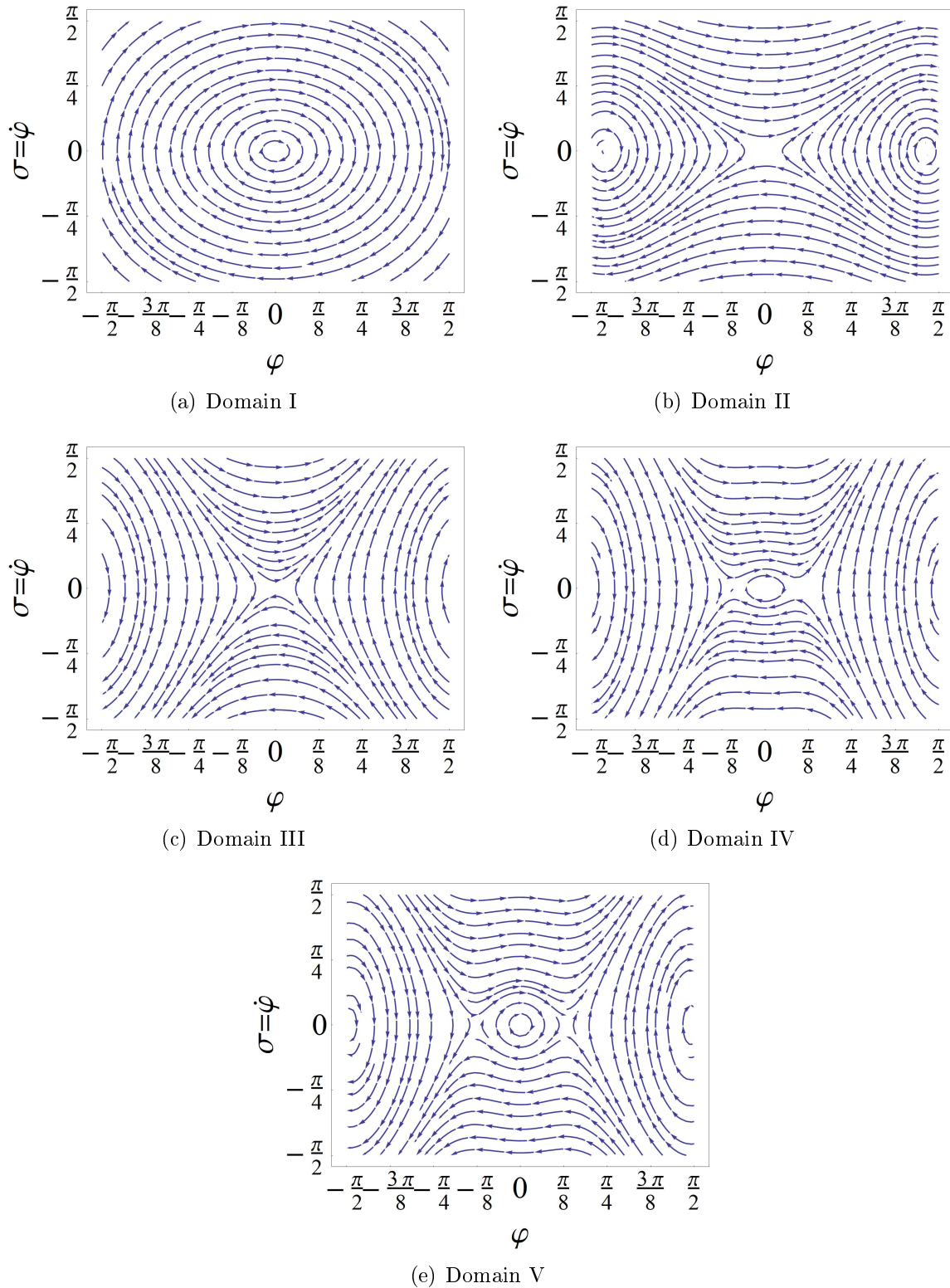


**Figure 2.8:** Structure of phase-space in specific domains

domain II or III (the difference between II and III is the same as it is between V and IV). The stability of the straight line motion will change if we reach domain II or III, it is not a centre any more, it is a saddle. This type of bifurcation is called *saddle-node* bifurcation. Domain II and III are not good cases from the skater's view point, because he will tilt until an outer equilibria, what can be too big, so the skater may fall.

If the origin is unstable (domain II or III) and the velocity increase then the straight line motion becomes stable, this effect of increasing velocity was known from Figure 2.4, as well.

The phase-space diagrams for  $a$  is not zero can be found in Appendix B. The numerical simulations for this model can be found in Appendix C. A solution with big perturbation can be also seen (Figure C.4).

### 2.2.6 Limit cycle

To study the existance of limit cycles the Bendixson criterion can be applied. If the so called *Bendixon function* ( $\mathcal{B}$ ) does not change sign, than there is no limit cycle. The definition of this function is

$$\mathcal{B}(\varphi, \sigma) := \frac{\partial \dot{\sigma}}{\partial \sigma} + \frac{\partial \dot{\varphi}}{\partial \varphi}. \quad (2.2.32)$$

In our case, this function is

$$\mathcal{B}(\varphi, \sigma) = -\alpha_V \theta_a \cos^2 \varphi \quad (2.2.33)$$

which is positive or zero for any  $\varphi$  and zero in only individual points not in a continuous domains. Thus limit cycles can not exist for any parameter set.

## 2.3 Comparing the models

The conservative approach models the unbacked skateboard better, whereas the non - conservative one assumes an active rider, who just keeps the longitudinal velocity on the same level and does not try to balance.

It can be seen, that the two models give the same linear stability criterion. This means both models can be used for investigations if the perturbations are small.

In addition, the non-linear equilibria have the same structure with exactly the same values. This can be seen in subsections 2.1.6 and 2.2.5.

Based on these, the behaviour of the skateboard can be analysed with the help of both models and they give the same results. For further investigation the nearly self-balancing skateboard model is going to be used, that is the model with the kinematic constraints relating to the longitudinal velocity, because the describing equations can be handled more easily.

So the *Controlled skateboard* model based on the nearly self-balancing skateboard model.

# Chapter 3

## Controlled skateboard

In this chapter the effect of the skater is analysed, which makes the mechanical model more complex than it was in Chapter 2. The skater is able to make torque between himself and the board and necessarily the skater and the board have their own degree of freedom, therefore the tilt of the skater and the board is not the same at any time. The two models in Chapter 2 give the same result in the linear case, thus in this section only the simpler model is investigated, which consists the uniform longitudinal velocity constraint.

After the construction of the equations of motion with the help of Appell-Gibbs method for arbitrary human control, we verify the equations of motion with the previous equations. If a rigid connection is supposed, then the equations of motion must be the same as in Chapter 2. After this verification the skater control is going to be modelled as a PD control loop. Finally the reflex time of the skater is going to be taken in the investigation.

### 3.1 Derivation of the equation of motion

In this section the equation of the motion is derived with the help of Appell-Gibbs equation. The model is constructed with arbitrary *control torque* ( $M_c$ ) by the skater, therefore any control loop can be applied in what follows.

#### 3.1.1 Mechanical model

The mechanical model (see Figure 3.1) is almost the same as before. The model consists the same elements: one mass point (C), two massless rods (RF and CS) and the torsional spring ( $s_t$ ), which are the same as in Chapter 2. There are two differences between the two models. First the two massless rods are not connected rigidly at point S and the second, there is a *control torque* between the skater and the board. The model parameters are the same.

A new generalised coordinate is necessary because of the new degree of freedom, this is the tilt of the board and it is denoted with  $\beta$ . This coordinate can be also seen in Figure 3.1. Therefore there are 5 generalised coordinates:  $X$ ,  $Y$ ,  $\psi$ ,  $\varphi$  and  $\beta$ .

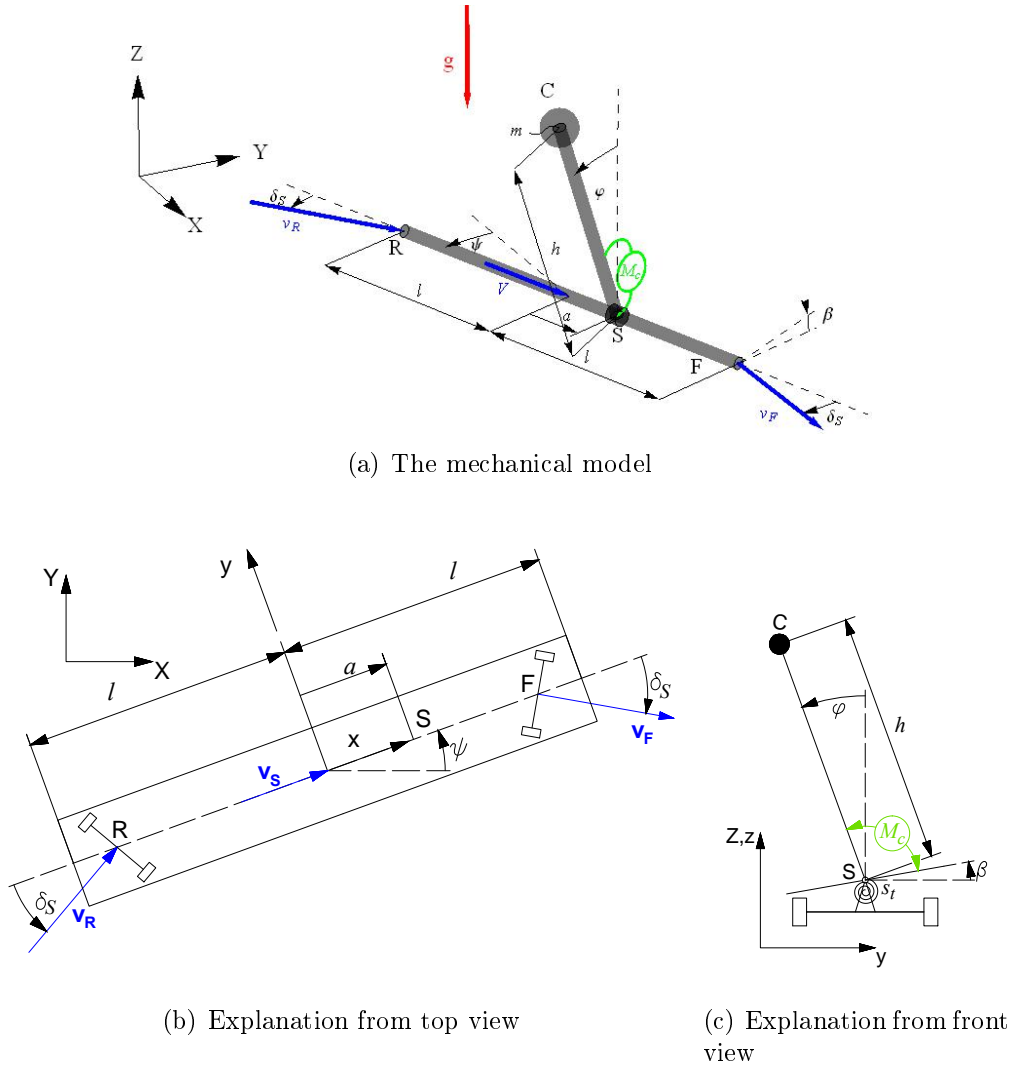


**Figure 3.1:** Mechanical model of the controlled skateboard

The structure of the kinematic constraint is the same as it was in Chapter 2 (2.2.2), but there the constraints were depended on  $\varphi$  and now they are dependent on  $\beta$ , because  $\beta$  represents the tilt of the board. Technically  $\varphi$  has to be substituted by  $\beta$ :

$$\mathbf{A} = \begin{bmatrix} -\sin \psi + \cos \psi \sin \beta \tan \kappa & \cos \psi + \sin \psi \sin \beta \tan \kappa & -a + l & 0 \\ \sin \psi + \cos \psi \sin \beta \tan \kappa & -\cos \psi + \sin \psi \sin \beta \tan \kappa & a + l & 0 \\ \cos \psi & \sin \psi & 0 & 0 \end{bmatrix} \quad (3.1.1)$$

and  $\mathbf{A}_0$  is the same:

$$\mathbf{A}_0 = \begin{bmatrix} 0 & 0 & -V \end{bmatrix}^T. \quad (3.1.2)$$

Naturally the kinematic constraints can be obtainable in the same way:

$$\mathbf{A}\dot{\mathbf{q}} + \mathbf{A}_0 = \mathbf{0}. \quad (3.1.3)$$

Anything else (e.g. acceleration of point C and etc.) is the same as in Chapter 2.

### 3.1.2 Equation of motion

There are 2 pseudo velocities required even though there are 3 kinematic constraints, but there is one more generalised coordinate too. The first pseudo velocity can be the relative angular velocity of the skater and the second one can be the relative angular velocity of the board:

$$\sigma := \dot{\varphi}, \quad (3.1.4a)$$

$$\nu := \dot{\beta}. \quad (3.1.4b)$$

In this case the generalised velocities in terms of the generalised coordinates and the pseudo velocities becomes:

$$\begin{bmatrix} \dot{X} \\ \dot{Y} \\ \dot{\psi} \\ \dot{\varphi} \\ \dot{\beta} \end{bmatrix} = \begin{bmatrix} V (\cos \psi + \frac{a}{l} \sin \beta \sin \psi \tan \kappa) \\ V (\sin \psi - \frac{a}{l} \sin \beta \cos \psi \tan \kappa) \\ -V \sin \beta \frac{\tan \kappa}{l} \\ \sigma \\ \nu \end{bmatrix}. \quad (3.1.5)$$

The energy of acceleration is created by the same method as in (2.1.32):

$$\frac{\mathcal{A}}{mh^2} = \left( \alpha_V \cos \varphi (\alpha_V \theta_h \sin \beta + \theta_a \nu \cos \beta) - \frac{1}{2} \alpha_V^2 \theta_h^2 \sin(2\varphi) \sin^2 \beta \right) \dot{\sigma} + \frac{1}{2} \dot{\sigma}^2 + \dots \quad (3.1.6)$$

The derivation of pseudo forces is complicated because of the control torque. The virtual power of the active forces is given by:

$$\delta P = \mathbf{G} \cdot \delta \mathbf{v}_C + \mathbf{M}_c \cdot \boldsymbol{\omega}_s + (-\mathbf{M}_c) \cdot \boldsymbol{\omega}_b + \mathbf{M}_{s_t} \cdot \delta \boldsymbol{\omega}_b, \quad (3.1.7)$$

where the expression of angular velocity of the skater  $\boldsymbol{\omega}_s$  is the same as the angular velocity

of the rigid body  $\omega$  in Chapter 2. The angular velocity vector of the board is

$$\omega_b = \begin{bmatrix} \dot{\beta} \cos \psi & \dot{\beta} \sin \psi & \dot{\psi} \end{bmatrix}^T \quad (3.1.8)$$

and the vector of the control torque is

$$\mathbf{M}_c = \begin{bmatrix} -M_c(t) \cos \psi & -M_c(t) \sin \psi & 0 \end{bmatrix}^T. \quad (3.1.9)$$

Evaluating expression (3.1.7) we find:

$$\begin{aligned} \delta P &= mgh \sin \varphi \delta \dot{\varphi} - M_c(t) \delta \dot{\varphi} + M_c(t) \delta \dot{\beta} - s_t \sinh \beta \delta \dot{\beta} = \\ &= (mgh \sin \varphi - M_c(t)) \delta \dot{\varphi} + (M_c(t) - s_t \sinh \beta) \delta \dot{\beta}. \end{aligned} \quad (3.1.10)$$

The coefficient of  $\delta \dot{\beta}$  is 0; this can be easily seen with the help of the free-body diagram of the system (see Figure 3.2). Therefore the board is massless and this is a static problem.

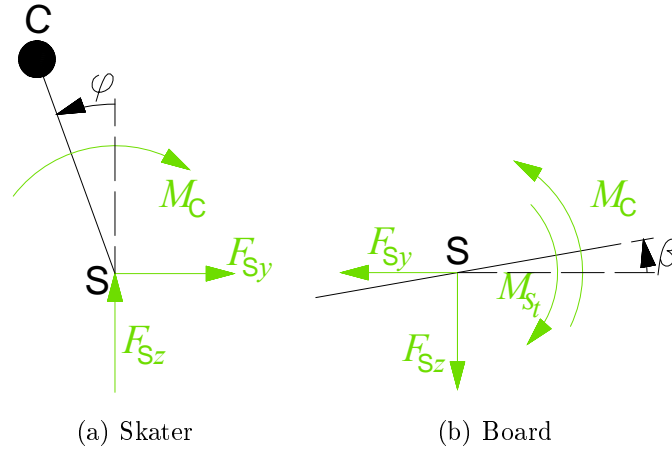


**Figure 3.2:** Free-body diagram of the controlled skateboard model in  $x - y$  plane

The torque equilibrium in this plane static problem is really simple:

$$0 = M_c(t) - s_t \sinh \beta, \quad (3.1.11)$$

which is the same as the coefficient of  $\delta \dot{\beta}$  in (3.1.10), so the virtual power is

$$\delta P = (mgh \sin \varphi - M_c(t)) \delta \dot{\varphi}. \quad (3.1.12)$$

From expression (3.1.12) the pseudo forces are given by

$$\frac{\Gamma}{mh^2} = \alpha_g^2 \sin \varphi - \alpha_{s_t}^2 m_c(t) \quad \text{and} \quad \frac{\Lambda}{mh^2} = 0, \quad (3.1.13)$$

where  $\Lambda$  is the pseudo force of  $\nu$  and

$$m_c(t) := \frac{M_c(t)}{s_t}. \quad (3.1.14)$$

Since the energy of acceleration (3.1.6) is independent on  $\nu$  and  $\Lambda$  is zero the Appell-Gibbs equation related to  $\nu$  is the trivial identity:

$$0 = 0, \quad (3.1.15)$$

therefore there is one equation less than required. But from the torque equilibrium (3.1.11) we find a connection between  $\beta$  and  $M_c$ :

$$\beta = \operatorname{arcsinh} \frac{M_c(t)}{s_t} = \operatorname{arcsinh}(m_c(t)). \quad (3.1.16)$$

The pseudo velocity  $\nu$  is given by:

$$\nu = \dot{\beta} = \frac{\dot{m}_c(t)}{\sqrt{1 + m_c^2(t)}}. \quad (3.1.17)$$

Thus the equations of the motion are:

$$\begin{aligned} \dot{\sigma} = & -\alpha_V \cos \varphi \left( \alpha_V \theta_h \sin(\operatorname{arcsinh}(m_c(t))) + \theta_a \frac{\dot{m}_c(t)}{\sqrt{1 + m_c^2(t)}} \cos(\operatorname{arcsinh}(m_c(t))) \right) \\ & + \frac{1}{2} \alpha_V^2 \theta_h^2 \sin(2\varphi) \sin^2(\operatorname{arcsinh}(m_c(t))) + \alpha_g^2 \sin \varphi - \alpha_{s_t}^2 m_c(t), \end{aligned} \quad (3.1.18a)$$

$$\dot{\varphi} = \sigma, \quad (3.1.18b)$$

$$\frac{\dot{X}}{h} = \alpha_V (\cos \psi + \theta_a \sin \psi \sin(\operatorname{arcsinh}(m_c(t)))) , \quad (3.1.18c)$$

$$\frac{\dot{Y}}{h} = \alpha_V (\sin \psi - \theta_a \cos \psi \sin(\operatorname{arcsinh}(m_c(t)))) , \quad (3.1.18d)$$

$$\dot{\psi} = -\alpha_V \theta_h \sin(\operatorname{arcsinh}(m_c(t))). \quad (3.1.18e)$$

Here the  $X$ ,  $Y$  and  $\psi$  coordinates are cyclic coordinates, and  $\beta$  is a function of  $M_c$ , so this is a known variable. These variables are not necessary for the further investigation of the system.

## 3.2 Rigid skater – board connection

In this section we are going to check the identity of the equations of motion (2.2.9) and (3.1.18) when the connection between the skater and the board is rigid.

The rigid connection means that the tilt of the board is the same as the leaning of the skater:

$$\beta = \varphi. \quad (3.2.1)$$

From (3.1.16) and (3.2.1) the control torque is given by:

$$m_c(t) = \sinh \varphi. \quad (3.2.2)$$

Equations (3.2.3) can be obtained with this simple control torque, which are exactly the same as equations (2.2.9). So the *self-balancing skateboard* model is a special case of the *controlled skateboard* model.

$$\dot{\sigma} = \alpha_g^2 \sin \varphi - \alpha_{st}^2 \sinh \varphi + \frac{1}{2} \alpha_V^2 \theta_h (\theta_h \sin^2 \varphi - 1) \sin(2\varphi) - \alpha_V \theta_a (1 - \sin^2 \varphi) \sigma, \quad (3.2.3a)$$

$$\dot{\varphi} = \sigma, \quad (3.2.3b)$$

$$\frac{\dot{X}}{h} = \alpha_V (\cos \psi + \theta_a \sin \varphi \sin \psi), \quad (3.2.3c)$$

$$\frac{\dot{Y}}{h} = \alpha_V (\sin \psi - \theta_a \sin \varphi \cos \psi), \quad (3.2.3d)$$

$$\dot{\psi} = -\alpha_V \theta_h \sin \varphi. \quad (3.2.3e)$$

### 3.3 Simple skater balancing

In this section we are going to model human balancing on a skateboard with a PD control loop.

#### 3.3.1 Equation of motion

The magnitude of the control torque is given by a PD controller:

$$M_c(t) = P\varphi + D\dot{\varphi}, \quad (3.3.1)$$

hence

$$m_c(t) = p\varphi + d\dot{\varphi}, \quad (3.3.2)$$

where

$$p = \frac{P}{s_t} \quad \text{and} \quad d = \frac{D}{s_t}. \quad (3.3.3)$$

With this control torque the first equation of (3.1.18a) becomes:

$$\begin{aligned} \dot{\sigma} = & \frac{1}{2}\alpha_V^2\theta_h^2 \sin(2\varphi) \sin^2(\operatorname{arcsinh}(p\varphi + d\sigma)) + \alpha_g^2 \sin \varphi - \alpha_{s_t}^2 (p\varphi + d\sigma) - \\ & - \alpha_V \cos \varphi \left( \alpha_V \theta_h \sin(\operatorname{arcsinh}(p\varphi + d\sigma)) + \theta_a \frac{p\sigma + d\dot{\sigma}}{\sqrt{1 + (p\varphi + d\sigma)^2}} \cos(\operatorname{arcsinh}(p\varphi + d\sigma)) \right) \end{aligned} \quad (3.3.4)$$

It can be seen, that there is a  $\dot{\sigma}$  on both sides of the equation. Thus the (first order) ordinary differential equations of the motion can be written as:

$$\dot{\sigma} = \frac{A_\sigma(\varphi, \sigma)}{B(\varphi, \sigma)}, \quad (3.3.5a)$$

$$\dot{\varphi} = \sigma, \quad (3.3.5b)$$

$$\frac{\dot{X}}{h} = \alpha_V (\cos \psi + \theta_a \sin \psi \sin(\operatorname{arcsinh}(p\varphi + d\sigma))), \quad (3.3.5c)$$

$$\frac{\dot{Y}}{h} = \alpha_V (\sin \psi - \theta_a \cos \psi \sin(\operatorname{arcsinh}(p\varphi + d\sigma))), \quad (3.3.5d)$$

$$\dot{\psi} = -\alpha_V \theta_h \sin(\operatorname{arcsinh}(p\varphi + d\sigma)). \quad (3.3.5e)$$

where

$$B(\varphi, \sigma) = 1 + \frac{\alpha_V \theta_a d}{\sqrt{1 + (p\varphi + d\sigma)^2}} \cos \varphi \cos(\operatorname{arcsinh}(p\varphi + d\sigma)) \quad (3.3.6)$$

and

$$A_\sigma(\varphi, \sigma) = \frac{1}{2} \alpha_V^2 \theta_h^2 \sin(2\varphi) \sin^2(\operatorname{arcsinh}(p\varphi + d\sigma)) - \alpha_V^2 \theta_h \cos \varphi \sin(\operatorname{arcsinh}(p\varphi + d\sigma)) \quad (3.3.7)$$

$$- \alpha_V \cos \varphi \theta_a \frac{p\sigma}{\sqrt{1 + (p\varphi + d\sigma)^2}} \cos(\operatorname{arcsinh}(p\varphi + d\sigma)) - \alpha_{st}^2 (p\varphi + d\sigma) + \alpha_g^2 \sin \varphi$$

The trivial solution is the static straight line motion, given by the following pseudo velocity and generalised coordinates:

$$\sigma = 0, \quad \varphi = 0, \quad X = Vt, \quad Y = 0 \quad \text{and} \quad \psi = 0, \quad (3.3.8)$$

these are the same as (2.2.10).

### 3.3.2 Linear stability analysis of the straight line motion

The linear system can be written in the same form as equation (2.1.40)

$$\dot{\mathbf{X}} = \mathbf{J}(\mathbf{X} - \mathbf{X}_0), \quad (3.3.9)$$

where

$$\mathbf{J} = \begin{bmatrix} -\frac{\alpha_V \theta_a p + (\alpha_{st}^2 + \alpha_V^2 \theta_h) d}{1 + \alpha_V \theta_a d} & \frac{\alpha_g^2 - (\alpha_{st}^2 + \alpha_V^2 \theta_h) p}{1 + \alpha_V \theta_a d} \\ 1 & 0 \end{bmatrix} \quad (3.3.10)$$

and  $\mathbf{X}$  and  $\mathbf{X}_0$  are the same as expression (2.2.19):

$$\mathbf{X} = \begin{bmatrix} \sigma \\ \varphi \end{bmatrix}, \quad \text{and} \quad \mathbf{X}_0 = \begin{bmatrix} 0 \\ 0 \end{bmatrix}. \quad (3.3.11)$$

The stability criteria can be derived with the help of Routh-Hurwitz theory, from the Jacobian matrix (3.3.10).

$$\frac{\alpha_V \theta_a p + (\alpha_{st}^2 + \alpha_V^2 \theta_h) d}{1 + \alpha_V \theta_a d} > 0, \quad (3.3.12a)$$

$$\frac{(\alpha_V \theta_a p + (\alpha_{st}^2 + \alpha_V^2 \theta_h) d) (\alpha_g^2 - (\alpha_{st}^2 + \alpha_V^2 \theta_h) p)}{(1 + \alpha_V \theta_a d)^2} > 0. \quad (3.3.12b)$$

The stability criteria with the original parameters can be written in the form of (3.3.13), if  $h$  and  $m$  are positive. The stability criteria (3.3.12) are equivalent to (3.3.13) if and only if

all of the expressions in (3.3.13) have the same sign.

$$aPmhV \tan \kappa + D (mhV^2 \tan \kappa + ls_t) \quad (3.3.13a)$$

$$aDV \tan \kappa + hls_t \quad (3.3.13b)$$

$$ls_t(P - mgh) + hmPV^2 \tan \kappa \quad (3.3.13c)$$

Thus there are two cases; all of the (3.3.13) expressions are positive or negative.

If all of the (3.3.13) are less than zero, the equilibrium under consideration is stable if the parameters are chosen from the grey domain in Figure 3.3. It means  $P$  is less than a critical value:

$$P_c = \frac{mgh}{1 + \frac{h}{l} \frac{mV^2}{s_t} \tan \kappa}, \quad p_c = \frac{\alpha_g^2}{\alpha_{s_t}^2 + \alpha_V^2 \theta_h}. \quad (3.3.14)$$

If all of the (3.3.13) are greater than zero, the equilibrium is stable if the  $P$  is chosen from the grey domain of Figure 3.4. In this case the parameter is greater than the critical value  $P_c$ .

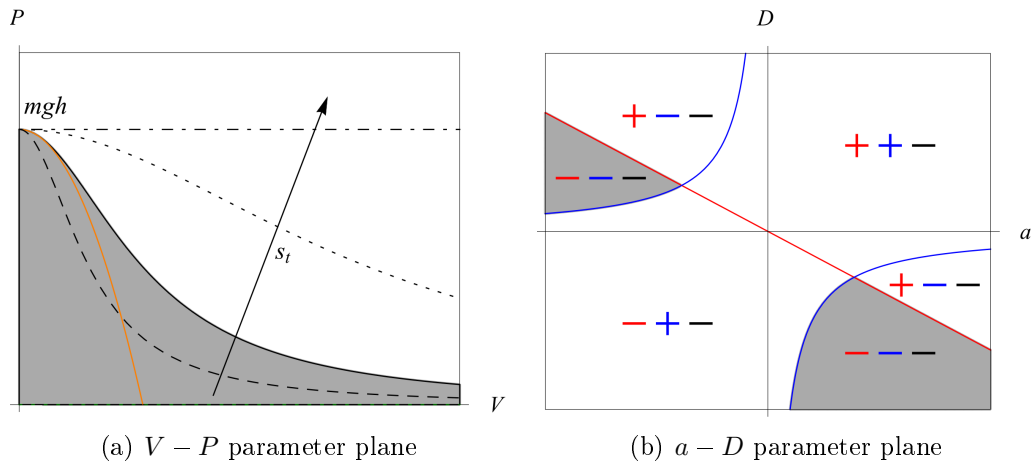


**Figure 3.3:** Explanation for stability charts of the PD controlled skateboard in case of all the expressions (3.3.13) are less than zero

This critical proportional parameter can be seen in Figure 3.3(a) and Figure 3.4(a) with different spring stiffnesses. These are the black lines, the dotted-dashed black line is related to the infinite spring stiffness. The orange line is related to the required spring stiffness ( $s_{t,c}$ ) in the *self-balancing skateboard* model. In Figure 3.3(b) and Figure 3.4(b) the red line means that expression (3.3.13a) is equal to zero and the + or - marks give the sign of this expression in the particular domains. The blue curve denotes where expression (3.3.13b) is zero and the + or - marks give the sign of the expression. The black marks denote the sign of the (3.3.13c) expression. As was mentioned the investigated equilibrium is stable if all of

the (3.3.13) expressions have the same sign; all negative (see in Figure 3.3) or positive (see in Figure 3.4).

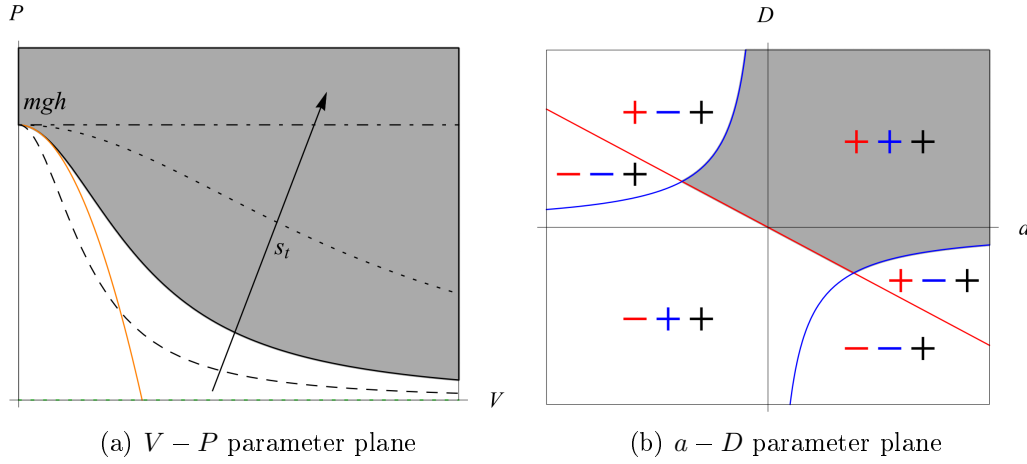


**Figure 3.4:** Explanation for stability charts of the PD controlled skateboard in case of all the expressions (3.3.13) are greater than zero

The effect of the torsion spring stiffness on the critical value of the proportional parameter is already known, but the effect of the proportional parameter and the longitudinal velocity on the  $a - D$  plane is unknown. Figure 3.5 can be used to understand these effects.

The gradient of the red line in Figure 3.3 and 3.4 decreases as the longitudinal velocity ( $V$ ) increases, then it begins to increase at

$$V = \sqrt{\frac{ls_t}{mh \tan \kappa}} \quad (3.3.15)$$

until it reaches 0 at  $V = \infty$ . The equation of the blue curve is:

$$D(a) = \frac{s_t hl}{V \tan \kappa a}, \quad (3.3.16)$$

thus as  $V$  increases this curve is asymptotes to the axes.

The changing of the proportional parameter has an effect of the red line's gradient only, if  $P$  increases then the gradient decreases and the connection between them is linear.

When the skateboard is not moving ( $V = 0$ ), the equilibrium can not be stable if the proportional parameter is less than the critical value ( $P_c$ ), as can be seen from the first row of Figure 3.5. It can be also seen that any  $a$  parameter can be chosen when  $V = 0$ , the equilibrium will be stable if  $D$  greater than zero and the  $P$  parameter is enough big. This is obvious, because if the board is not moving than there is no front part and rear part as it was mentioned in the previous chapter, Chapter 2.

If the longitudinal velocity would be infinite, the structure of the stability charts do not depend on other parameters. The motion will be stable only with positive  $P$ ,  $D$  and  $a$  parameters.

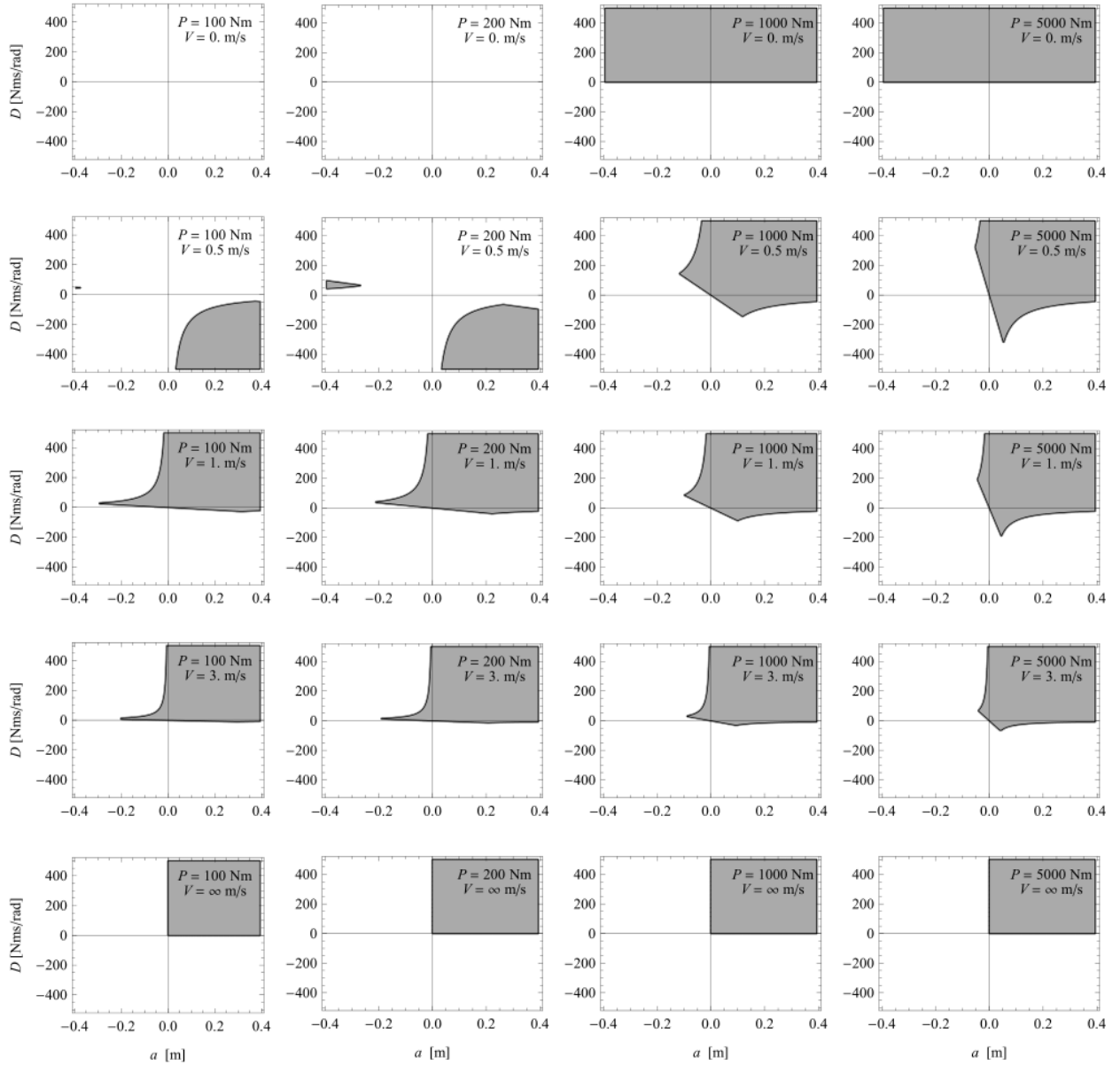


**Figure 3.5:** Stability charts of the PD controlled skateboard with the effect of changing the proportional parameter and the longitudinal velocity

Compared with the *self-balancing skateboard* model, it can be said, that the PD controller expands the stable domain, therefore this PD control loop is not able to cause the loss of stability at higher speed.

Numerical simulations can be found in Appendix D for stable and unstable cases too.

## 3.4 Riding on skateboard with reflex time

The consideration of human control can not be completed without the reflex time of the skater, inasmuch as the time delay plays a significant role in the stability of mechanical systems, for example in robotics and machine tool vibrations (Stépán, 1989). The time delay in mechanical systems is able to change the stability behaviour, even stabilize an unstable equilibrium or even contrariwise. In this section a PD controller is used to model the interaction of the skater and the board, but there is also a delay in the control loop.

### 3.4.1 Equation of motion

In this case the magnitude of the control torque is similar to the control torque in equation (3.3.1):

$$M_c(t) = P\varphi(t - \tau) + D\dot{\varphi}(t - \tau), \quad (3.4.1)$$

this means

$$m_c(t) = p\varphi(t - \tau) + d\dot{\varphi}(t - \tau). \quad (3.4.2)$$

The equations of the motion with this control are

$$\begin{aligned} \dot{\sigma} = & \frac{1}{2}\alpha_V^2\theta_h^2 \sin(2\varphi) \sin^2(\operatorname{arcsinh}(p\varphi(t - \tau) + d\sigma(t - \tau))) - \alpha_{s_t}^2 (p\varphi(t - \tau) + d\sigma(t - \tau)) + \\ & + \alpha_g^2 \sin \varphi - \alpha_V^2\theta_h \cos \varphi \sin(\operatorname{arcsinh}(p\varphi(t - \tau) + d\sigma(t - \tau))) - \\ & - \alpha_V\theta_a \frac{p\sigma(t - \tau) + d\dot{\sigma}(t - \tau)}{\sqrt{1 + (p\varphi(t - \tau) + d\sigma(t - \tau))^2}} \cos \varphi \cos(\operatorname{arcsinh}(p\varphi(t - \tau) + d\sigma(t - \tau))) \end{aligned} \quad (3.4.3a)$$

$$\dot{\varphi} = \sigma, \quad (3.4.3b)$$

$$\frac{\dot{X}}{h} = \alpha_V (\cos \psi + \theta_a \sin \psi \sin(\operatorname{arcsinh}(p\varphi(t - \tau) + d\sigma(t - \tau)))) , \quad (3.4.3c)$$

$$\frac{\dot{Y}}{h} = \alpha_V (\sin \psi - \theta_a \cos \psi \sin(\operatorname{arcsinh}(p\varphi(t - \tau) + d\sigma(t - \tau)))) , \quad (3.4.3d)$$

$$\dot{\psi} = -\alpha_V\theta_h \sin(\operatorname{arcsinh}(p\varphi(t - \tau) + d\sigma(t - \tau))). \quad (3.4.3e)$$

This system is a neutral delay differential equation system, if neither  $\theta_a$  nor  $\alpha_V$  is zero. The first two equations can be decoupled from the last three ones, namely the generalised coordinates  $X$ ,  $Y$  and  $\psi$  are cyclic coordinates here too. Also the trivial equilibrium is not changed, this is the same as in expression (3.3.8).

### 3.4.2 Linear stability analysis of the straight line motion

The linear delayed differential equation system can be written in the

$$\dot{\mathbf{X}}(t) = \mathbf{J}\mathbf{X}(t) + \mathbf{T}_0\mathbf{X}(t - \tau) + \mathbf{T}_1\dot{\mathbf{X}}(t - \tau), \quad (3.4.4)$$

form, where

$$\mathbf{J} = \begin{bmatrix} 0 & \alpha_g^2 \\ 1 & 0 \end{bmatrix}, \quad \mathbf{T}_0 = \begin{bmatrix} -\alpha_V\theta_a p - (\alpha_{st}^2 + \alpha_V^2\theta_h) d & -(\alpha_{st}^2 + \alpha_V^2\theta_h) p \\ 0 & 0 \end{bmatrix} \quad (3.4.5)$$

and

$$\mathbf{T}_1 = \begin{bmatrix} -\alpha_V\theta_a d & 0 \\ 0 & 0 \end{bmatrix}. \quad (3.4.6)$$

The substitution of the trivial solution of the linear equation (3.4.4)

$$\mathbf{X}(t) = \begin{bmatrix} \sigma(t) \\ \varphi(t) \end{bmatrix} = \mathbf{K}e^{\lambda t}, \quad \mathbf{K} \in \mathbb{C}^2, \quad \lambda \in \mathbb{C} \quad (3.4.7)$$

leads to the characteristic function

$$D(\lambda) = (\alpha_V\theta_a d e^{-\lambda\tau} + 1) \lambda^2 + (\alpha_{st}^2 d + \alpha_V\theta_a p + \alpha_V^2\theta_h d) e^{-\lambda\tau} \lambda + (\alpha_{st}^2 + \alpha_V^2\theta_h) p e^{-\lambda\tau} - \alpha_g^2, \quad (3.4.8)$$

and the characteristic equation can be written in the form

$$D(\lambda) = 0. \quad (3.4.9)$$

Usually, there are infinitely many complex roots of the characteristic equation (3.4.9), but not all of the roots are situated in the right-half complex plane generally. The investigated equilibrium, in this case the stationary straight motion, is asymptotically stable if and only if all of the characteristic exponents are situated in the right-half complex plane (Stépán, 1989). The limit of stability is where the characteristic roots are located at the imaginary axis for some particular system parameters (e.g.:  $\alpha_g, \alpha_V, \dots$ ).

If not only the real part of the characteristic exponent is zero, but also the imaginary part of it is zero (so  $\lambda = 0$ ), then the bifurcation is called *saddle-node* (SN) bifurcation. In our case:

$$D(\lambda = 0) = (\alpha_{st}^2 + \alpha_V^2\theta_h) p - \alpha_g^2. \quad (3.4.10)$$

This type of bifurcation is also called *static loss of stability*, the critical dimensionless proportional parameter can be calculated from the characteristic equation ( $D(\lambda = 0) = 0$ ):

$$p_{\text{SN}} = \frac{\alpha_g^2}{\alpha_{st}^2 + \alpha_V^2 \theta_h}, \quad \tilde{p}_{\text{SN}} = 1. \quad (3.4.11)$$

This critical proportional parameter value decreases, while  $\alpha_V$  increases, it goes to zero, while  $\alpha_V$  goes to infinity.

If the real part of the characteristic exponent is zero and the imaginary part is not zero then a Hopf bifurcation may occur. In this case the characteristic exponent can be written as imaginary numbers:

$$\lambda_{1,2} = \pm i\omega, \quad \omega \in \mathbb{R}^+. \quad (3.4.12)$$

A complex equation is obtained at the boundary of stability from equation (3.4.12); separating this into real and imaginary parts, we arrive at:

$$0 = ((\alpha_{st}^2 + \alpha_V^2 \theta_h) p - \alpha_V \theta_a d \omega^2) \cos(\omega\tau) + ((\alpha_{st}^2 + \alpha_V^2 \theta_h) d + \alpha_V \theta_a p) \omega \sin(\omega\tau) - \alpha_g^2 - \omega^2, \quad (3.4.13a)$$

$$0 = ((\alpha_{st}^2 + \alpha_V^2 \theta_h) d + \alpha_V \theta_a p) \omega \cos(\omega\tau) - ((\alpha_{st}^2 + \alpha_V^2 \theta_h) p - \alpha_V \theta_a d \omega^2) \sin(\omega\tau), \quad (3.4.13b)$$

The following dimensionless parameters are introduced:

$$\tilde{\tau} = \tau \alpha_g, \quad \tilde{\omega} = \frac{\omega}{\alpha_g}, \quad \tilde{p} = p \frac{\alpha_{st}^2 + \alpha_V^2 \theta_h}{\alpha_g^2}, \quad \tilde{d} = d \alpha_V \theta_a \quad \text{and} \quad r = \frac{\alpha_{st}^2 + \alpha_V^2 \theta_h}{\alpha_V \theta_a} \quad (3.4.14)$$

Equations (3.4.13) lead to

$$0 = (\tilde{p} - \tilde{d}\tilde{\omega}^2) \cos(\tilde{\omega}\tilde{\tau}) + \left(r\tilde{d} + \frac{\tilde{p}}{r}\right) \tilde{\omega} \sin(\tilde{\omega}\tilde{\tau}) - \tilde{\omega}^2 - 1, \quad (3.4.15a)$$

$$0 = \left(r\tilde{d} + \frac{\tilde{p}}{r}\right) \tilde{\omega} \cos(\tilde{\omega}\tilde{\tau}) - (\tilde{p} - \tilde{d}\tilde{\omega}^2) \sin(\tilde{\omega}\tilde{\tau}) \quad (3.4.15b)$$

with the new parameters.

The  $\tilde{\omega}\tilde{\tau}$  product can be eliminated from the equations (3.4.15), leading to an equation for the dimensionless frequency ( $\tilde{\omega}$ ):

$$\left(\tilde{p} - \tilde{d}\tilde{\omega}^2\right)^2 + \left(r\tilde{d} + \frac{\tilde{p}}{r}\right)^2 \tilde{\omega}^2 = (\tilde{\omega}^2 + 1)^2 \quad (3.4.16)$$

This is a quadratic equation for  $\tilde{\omega}^2$ , which can be written in the following form:

$$o_2 (\tilde{\omega}^2)^2 + o_1 \tilde{\omega}^2 + o_0 = 0, \quad (3.4.17)$$

where

$$o_2 = \tilde{d}^2 - 1, \quad o_1 = \frac{\tilde{p}^2}{r^2} + r^2 \tilde{d}^2 - 2 \quad \text{and} \quad o_0 = \tilde{p}^2 - 1. \quad (3.4.18)$$

Hence

$$\tilde{\omega}_{\pm}^2 = \frac{-o_1 \pm \sqrt{o_1^2 - 4o_0o_2}}{2o_2}. \quad (3.4.19)$$

There can be either zero, one (repeated) or two real positive roots, depending on the parameters; these results can be seen in Table 3.1. The sign of the coefficients of powers of  $\tilde{\omega}^2$  is in the first three columns, the sign of the expression under the root sign is in column four, the fifth column contains the number of solutions and the sixth column gives information about which combinations of signs are possible with the system parameters. When the sign in column four is  $\pm$  it means that the expression under the root sign can be also positive and negative, going a further condition.

The number of positive solutions for  $\tilde{\omega}^2$  equals to the number of positive solutions for  $\tilde{\omega}$  and here we only investigate the case where  $\tilde{\omega}$  is positive (the same real and imaginary part of the characteristic equation is obtained with positive or negative characteristic exponent so only positive  $\tilde{\omega}$  needs to be investigated).

**Table 3.1:** Number of positive solutions for  $\tilde{\omega}^2$

$o_2$	$o_0$	$o_1$	$o_1^2 - 4o_0o_2$	Nb. of sol.	Existence	Domain nb.
+	+	+	$\pm$	0	—	—
+	+	—	$\pm$	2 ( $\pm$ )	$\nexists$	—
+	—	$\pm$	+	1 (+)	$\exists$	I
—	+	$\pm$	+	1 (—)	$\exists$	II
—	—	+	$\pm$	2 ( $\pm$ )	$\exists$	III
—	—	—	$\pm$	0	—	—

This is easy to show, that the case in the second row is not possible; the first two conditions ( $o_2$  and  $o_0$  are greater than zero) leads to the

$$\tilde{d}^2 > 1 \quad \text{and} \quad \tilde{p}^2 > 1. \quad (3.4.20)$$

The condition that  $o_1 < 0$  can be written as

$$\frac{\tilde{p}^2}{r^2} + r^2 \tilde{d}^2 < 2. \quad (3.4.21)$$

If the smallest  $\tilde{p}$ ,  $\tilde{d}$  parameters are substituted in this inequality then a contradiction is given:

$$(r^2 - 1)^2 < 0. \quad (3.4.22)$$

It means that the left side of the inequality (3.4.21) can not be satisfied for any possible  $p$  and  $d$  parameters; this is the reason why there is a  $\#$  mark in Table 3.1.

The three domains, from the Table 3.1, can be seen in Figure 3.6, where the horizontal axes is  $\tilde{p}^2$  and the vertical axes is  $\tilde{d}^2$ . The continuous line correspondent to  $r^2 = 0.25$ , the dashed line to  $r^2 = 0.1$  and the dashed dotted line to  $r^2 = 5$ . It is easy to see that the curve

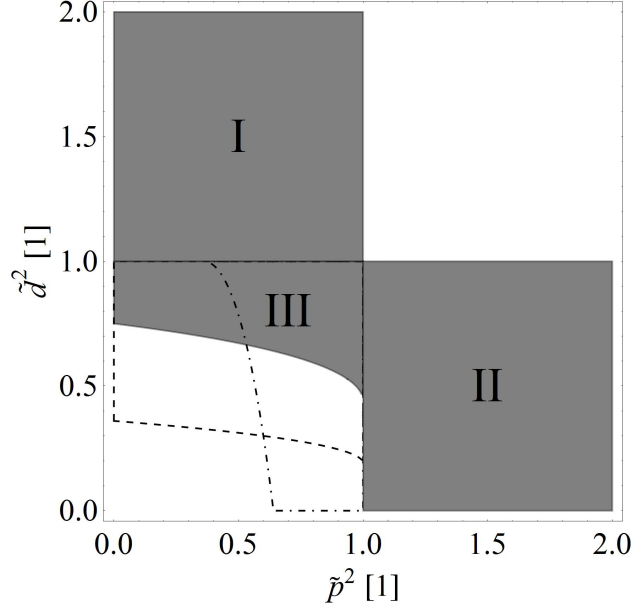


**Figure 3.6:** Number of positive solutions for  $\tilde{\omega}$  (and also  $\tilde{\omega}^2$ )

of the Hopf stability boundary can cross itself only if both  $|\tilde{p}| < 1$  and  $|\tilde{d}| < 1$ .

We can get an explicit expression for the time delay ( $\tau$ ) from the equations system (3.4.13) in terms of  $\tilde{\omega}_{\pm}$ :

$$\tilde{\tau} = \frac{1}{\tilde{\omega}_{\pm}} \left( \arctan \frac{\tilde{p} + r\tilde{d}}{\frac{\tilde{p}}{\tilde{\omega}_{\pm}} + \tilde{\omega}_{\pm}\tilde{d}} + k\pi \right), \quad k \in \mathbb{N} \quad (3.4.23)$$

Not only are  $\tilde{\omega}$  and  $\tilde{\tau}$  obtainable from equations (3.4.15);  $\tilde{p}$  and  $\tilde{d}$  can also be found:

$$\tilde{p}_H = \frac{r(1 + \tilde{\omega}^2)(r \cos(\tilde{\omega}\tilde{\tau}) + \tilde{\omega} \sin(\tilde{\omega}\tilde{\tau}))}{r^2 + \tilde{\omega}^2}, \quad (3.4.24a)$$

$$\tilde{d}_H = \frac{(1 + \tilde{\omega}^2)(-\tilde{\omega} \cos(\tilde{\omega}\tilde{\tau}) + r \sin(\tilde{\omega}\tilde{\tau}))}{\tilde{\omega}(r^2 + \tilde{\omega}^2)}. \quad (3.4.24b)$$

The saddle-node bifurcation can be interpreted as a vertical line at  $\tilde{p} = \tilde{p}_{SN}$  in the  $\tilde{p} - \tilde{d}$  parameter plane. The left half-plane from this vertical line is naturally unstable, because of the so called *static stability criteria*. Of course this vertical line consists the starting point

of the dynamical stability boundary:

$$\tilde{p}_{H,0} = \tilde{p}_H|_{\tilde{\omega}=0} = \tilde{p}_{SN} = 1, \quad \tilde{d}_{H,0} = \tilde{d}_H|_{\tilde{\omega}=0} = \frac{r\tilde{\tau} - 1}{r^2}. \quad (3.4.25)$$

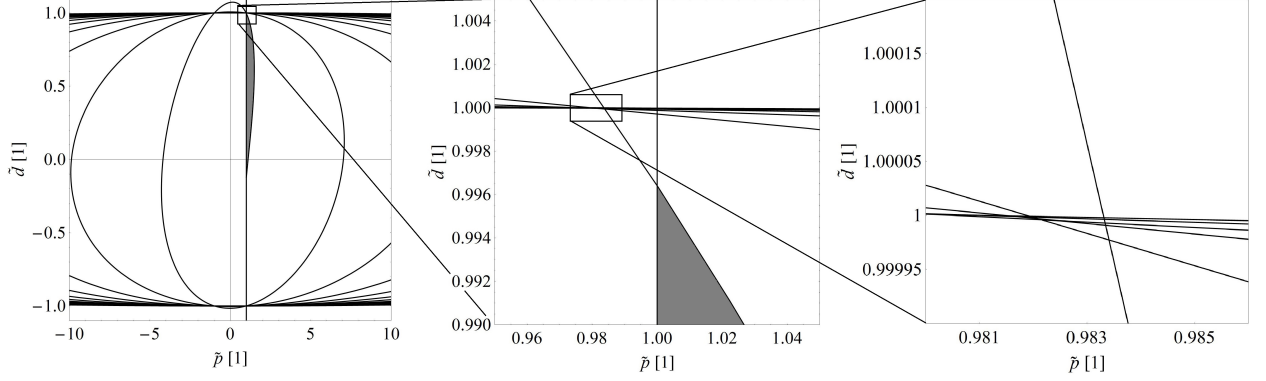


**Figure 3.7:** Structure of the stability chart of the PD controlled skateboard with the skater's reflex time

The structure of the stability chart of the static straight line motion can be seen in Figure 3.7. We can show, that

$$\tilde{p}_{H,\infty} = \lim_{\tilde{\omega} \rightarrow \infty} \tilde{p}_H = \tilde{\omega} \sin(\tilde{\omega}\tilde{\tau}) \quad \text{and} \quad \tilde{d}_{H,\infty} = \lim_{\tilde{\omega} \rightarrow \infty} \tilde{d}_H = -\cos(\tilde{\omega}\tilde{\tau}), \quad (3.4.26)$$

so the curve of the stability boundary goes to an ellipse whose centre is the origin, major axis is infinitely large and minor axis is 1, the equation of this ellipse is

$$\frac{\tilde{p}_H^2}{\tilde{\omega}^2} + \frac{\tilde{d}_H^2}{1} = 1. \quad (3.4.27)$$

If  $r$  less than  $\sqrt{2}$  then the minor axis is approached from larger values, otherwise it is approached from lower values; the major axis is approached from lower values regardless of the inequality.

In the next few paragraphs the effect of the skater's reflex time is investigated. If the  $\tilde{p}_H - \tilde{d}_H$  curve gives to the left side of the vertical line from the  $\tilde{p}_{H,0} - \tilde{d}_{H,0}$  point on the  $\tilde{p} - \tilde{d}$  parameter plane then there will not be any stable domain. Thus the necessary and sufficient condition for the existence of a stable domain is

$$\frac{d^2 \tilde{p}_H}{d\tilde{\omega}^2} = 2 - \frac{2}{r^2} + \frac{2\tilde{\tau}}{r} - \tilde{\tau}^2 > 0. \quad (3.4.28)$$

In Figure 3.8 , the grey domain indicates where the expression (3.4.28) is satisfied, so there is a stable domain in the  $\tilde{p} - \tilde{d}$  parameter plane.

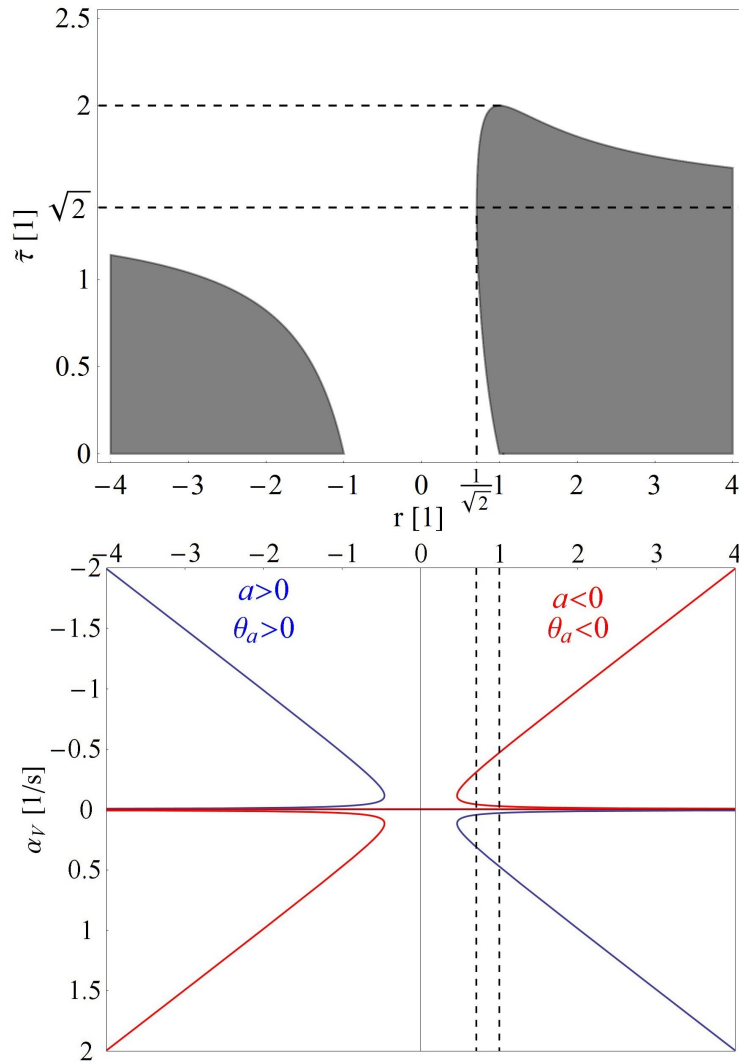


**Figure 3.8:** Critical time delay

There is a critical time delay ( $\tilde{\tau}_c, \tau_c$ ); if  $\tilde{\tau}$  is more than 2, then the investigated equilibrium will not be stable (the numerical value computed by the data of Table 2.1):

$$\tilde{\tau}_c = 2, \quad \tau_c = \frac{\tilde{\tau}_c}{\alpha_g} = \frac{2}{\alpha_g} = \frac{T_g}{\pi} \cong 0.588715 \quad [\text{s}], \quad (3.4.29)$$

where  $\alpha_g$  is the natural circular frequency of the uncontrolled skateboard and  $T_g$  is the period of time of the uncontrolled skateboard. This numerical value is close to the human reflex time, so we can say people with better reflexes can ride on a skateboard, while others not.

The effect of the velocity ( $\alpha_V$ ) on parameter  $r$  is shown in Figure 3.8. The parameter values are:  $\alpha_{st} = 0.2$  [1/s],  $\alpha_g = 3$  [1/s],  $\theta_a = \pm 0.5$  [1] and  $\theta_h = 3$  [1]. This example also illustrates well, that the equilibrium is stable at low velocity, then it becomes unstable,

finally it becomes stable again as the velocity ( $V$ ) increases. It does not appear that the minimum of parameter  $r$  ( $r_{\min}$ ) is grater than 1, namely

$$r_{\min} = 2 \frac{\alpha_{s_t} \sqrt{\theta_h}}{\alpha_g \theta_a} = 2 \sqrt{\frac{s_t}{mga}} \frac{1}{\sqrt{\frac{a}{l} \tan \kappa}} > 1. \quad (3.4.30)$$

It means  $s_t$  must be greater than a critical value:

$$s_t > \tilde{s}_{t,c} = \frac{1}{4} mga \frac{a}{l} \tan \kappa, \quad (3.4.31)$$

this critical value is small in reality, it can be shown in Figure 3.9. The maximum value of this spring stiffness is 142.125 [Nm] if  $a = l$ , but the parameter  $a$  is much smaller usually. Thus this not caves problems in the real world.

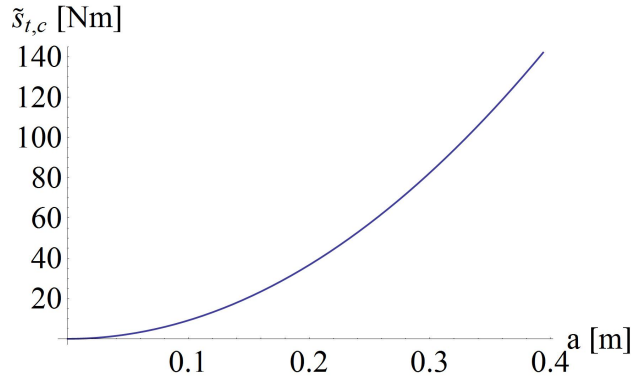


**Figure 3.9:** Critical spring stiffness for stable domain

In the following we investigate the effect of the velocity on another aspect of skateboarding. Parameter  $r$  decreases while the velocity ( $V$  and  $\alpha_V$ ) increases until it reaches  $V^*$  (or  $\alpha_V^*$ ):

$$\alpha_V^* = \frac{\alpha_{s_t}}{\sqrt{\theta_h}}, \quad V^* = \frac{s_t}{mh} \frac{1}{\sqrt{\frac{h}{l} \tan \kappa}}, \quad (3.4.32)$$

then this relation changes, parameter  $r$  will increase while the velocity continues to grow. Furthermore, if  $r$  decreases then the existing stable domain will decrease as well. This means, while the velocity is increasing then the stable domain increases too until the velocity reaches  $V^*$ , then it will decrease; this can be followed in Figure 3.10. In the dimensionless case the vertical line represents the saddle-node bifurcation and the other curves represent the Hopf-bifurcations; all of the  $D$ -shaped domains are stable even though only one is greyed out for the better visibility.

As shown in Figure 3.8 or 3.10, two velocities is related to each  $r$  (except at  $r_{\min}$ ). The parameters from Table 2.1 and 3.2 are used for stability chart 3.10 and 3.11.

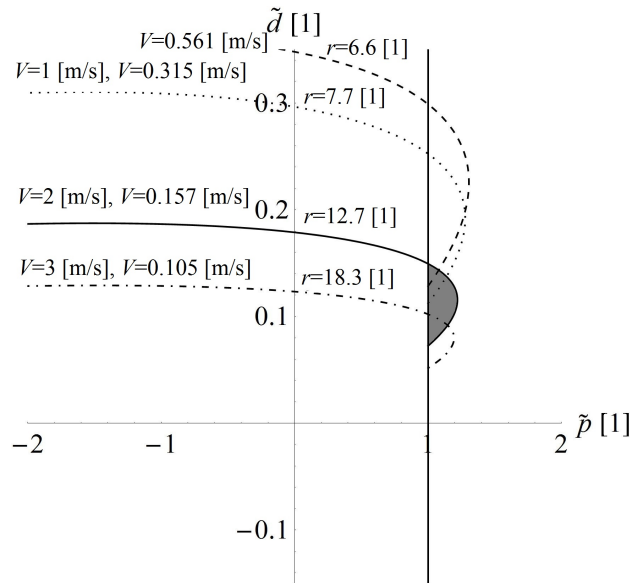


**Figure 3.10:** Dimensionless stability charts of the PD controlled skateboard with the skater's reflex time

**Table 3.2:** Parameters for the stability charts

$s_t$	$a$	$\tau$
[m]	[Nm]	[s]
100	0.05	0.294

The connection between the size of the stable domain and the velocity in the dimensional case is not the same as it was in the dimensionless case (see Figure 3.11). By increasing the velocity the size of the stable domain decreases and it also moves to the left and down. The latter one can be seen from the starting point of the Hopf-stability boundary (see expressions (3.4.25)). All of the D-shaped domains are stable in Figure 3.11 too, not only the greyed out one.

This behaviour of the stable domain is capable of illuminating the loss of stability at high speed. If we take into account a more complex connection between the skater and the board than a rigid one and we take into consideration the reflex time of the rider we could model the loss of stability at high speed.

The static straight motion can be stable for negative velocities too (this is equivalent to the negative value for parameter  $a$ ), but in this case the stable domains are smaller on the  $P$ - $D$  plane, and the required time delay is less than the other case (see the left side of Figure 3.8). But the impact of speed changes is the same, so if velocity goes to zero then the stable domain will increase. Thus negative velocity (or  $a$ ) makes worse conditions for stability.

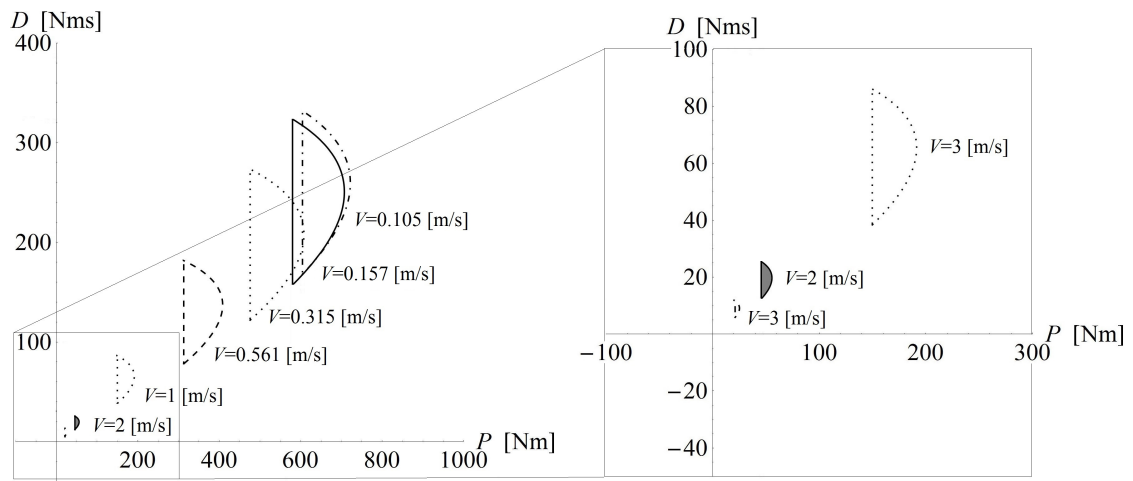


**Figure 3.11:** Stability charts of the PD controlled skateboard with the skater's reflex time

Numerical simulations can be found in Appendix E for stable and unstable cases too.

# Chapter 4

## Summary

The aim of this thesis is to find a reason why skateboarding is dangerous, what causes the instability at high speed. To understand this phenomenon we have created basically two different models, the first is the *self-balancing skateboard* and the second one is the *controlled skateboard*.

With the help of the *self-balancing skateboard* model we were not able to reach the goal of this project, but it has become clear that the constant velocity constraint has no effect on the linear stability of the static straight line motion or on the equilibria. Thus this simpler model can be used in further investigation. There is a negative effect of the higher velocity in the case of large perturbations, but to see it an unrealistically big perturbation is required.

The second model was unable to explain the adverse effect on the speed, when the skater was modelled with a simple PD controller. By accounting for the reflex time of the skater it can be explained. This model is only describable with delayed differential equations of the neutral type, which requires a more complicated mathematical method than the previous ordinary differential equations.

From this model we got a good quantitative result too, this is the value of the critical time delay (or reflex time  $t_c$ ), whose value is around 0.6 second. The human reaction time also falls in this range.

# Bibliography

- F. GANTMACHER : *Lectures in Analytical Mechanics*. MIR Publiser, Moscow, 1975.
- M. HUBBARD : Lateral dynamics and stability of the skateboard. *Journal of Applied Mechanics*, 46:931–936, December 1979.
- M. HUBBARD : Human control of the skateboard. *Journal of Biomechanics*, 13:745–754, 1980.
- T. INSPERGER and G. STÉPÁN : *Semi-Discretization for Time-Delay Systems*. Springer, 2011.
- Y. G. ISPOLOV and B. A. SMOLNIKOV : Skateboard dynamics. *Computer Methods in Applied Mechanics and Engineering*, 131:327–333, 1996.
- J. D. G. KOOLIJMAN, J. P. MEIJAARD, J. M. PAPADOPOULOS, A. RUINA and A. L. SCHWAB : A bicycle can be self-stable without gyroscopic or caster effects. *Science*, 332:339–342, 2011.
- A. V. KREMNEV and A. S. KULESHOV : Nonlinear dynamics and stability of a simplified skateboard model. Lomosow Moscow State University.
- A. V. KREMNEV and A. S. KULESHOV : Dinamics and simulation of the simplest model of a skateboard. In *ENOC-2008*, Saint Petersburg, Russia, June 2008.
- J. E. MARSDEN and M. MCCRACKEN : *The Hopf Bifurcation and Its Applications*. Sringer-Verlag New York, 1976.
- A. E. ÖSTERLING : MAS303 - on the skateboard, kinematics and dynamics. Not published, University of Exter, May 2004.
- G. STÉPÁN : *Retarded Dynamical Systems: Stability and Characteristic Functions*. Longman Scientific & Technical, 1989.

SZABADBAN.HU : A gördeszkázás története, 2013. URL <http://www.szabadban.hu/cikk.php?aid=d0c67e50cee0d22f53b4840>. Accessed: 2013.09.30.

M. WISSE and A. L. SCHWAB : Skateboard, bicycles, and three-dimensional biped walking machines: Velocity-dependent stability by means of lean-to-yaw coupling. *The International Journal of Robotics Research*, 24(6):417–429, June 2005.

YOUTUBE : Extreme skateboarding fall, 2013a. URL <http://www.youtube.com/watch?v=CCEqo2C1qtg>. Accessed: 2013.09.30.

YOUTUBE : Fail like a boss – EPIC, 2013b. URL [http://www.youtube.com/watch?v=5nTAn6E\\_f1E](http://www.youtube.com/watch?v=5nTAn6E_f1E). Accessed: 2013.09.30.

YOUTUBE : How not to go down the big hill, 2013c. URL [http://www.youtube.com/watch?v=adQbA\\_d0UVM&feature=related](http://www.youtube.com/watch?v=adQbA_d0UVM&feature=related). Accessed: 2013.09.30.

YOUTUBE : skateboarding over 40mph death, 2013d. URL <http://www.youtube.com/watch?v=zrgTeqofYfQ&feature=related>. Accessed: 2013.09.30.

# Appendix A

## Numerical simulations for the totally self-balancing skateboard

Numerical simulations for ordinary differential equation system (2.1.38) can be found in Appendix A. The numerical simulations is computed by the *ode45* function of MATLAB *2012b* software.

The values used for the parameters, which are not the same for all simulations, can be found in the table before the result of numerical simulations. The other parameters are the same for every numerical solution and they can be found in Table 2.1.

The so-called *energy error* ( $E_{\text{err}}$ ) function is computed from

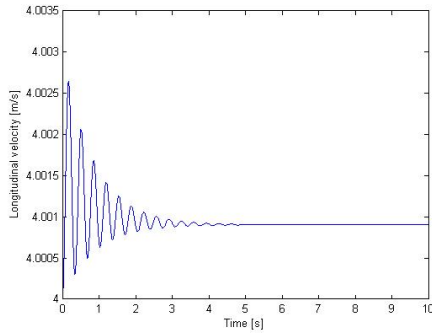
$$E_{\text{err}}(t) := \frac{E_t(t) - E_t(0)}{E_t(0)}. \quad (\text{A.0.1})$$

The order of this energy error is small, depending on the step size of the numerical method. If the step size decreases the energy error decreases as well.

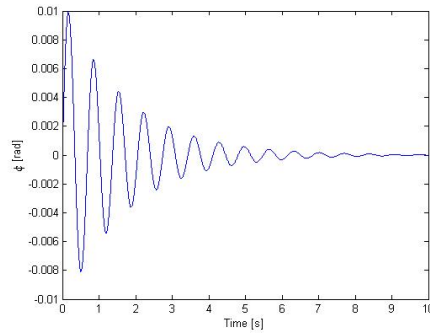
The simulation is unrealistic if  $|\varphi| > \pi/2$ , but it shows well the stability.

**Table A.1:** Values of parameters and initial conditions for totally self-balancing skateboard in the stable case

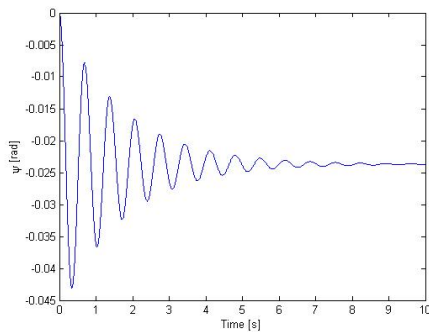
$s_t$	$a$	$\rho(0)$	$\sigma(0)$	$\varphi(0)$	$X(0)$	$Y(0)$	$\psi(0)$
[Nm]	[m]	[m/s]	[rad/s]	[rad]	[m]	[m]	[rad]
100	0.05	4	0.1	0	0	0	0



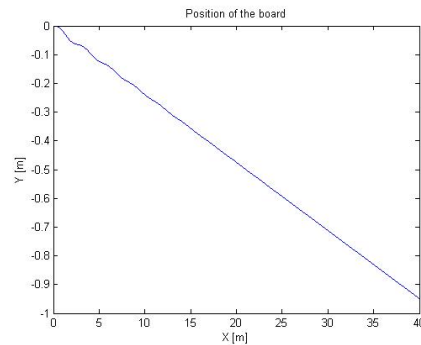
(a) Longitudinal velocity



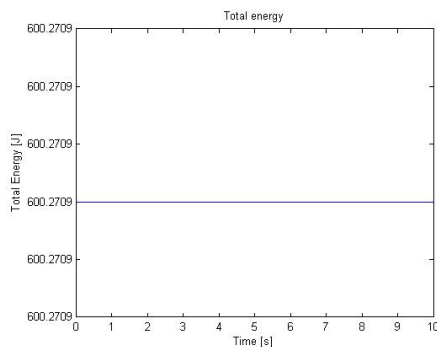
(b) Angle  $\varphi$



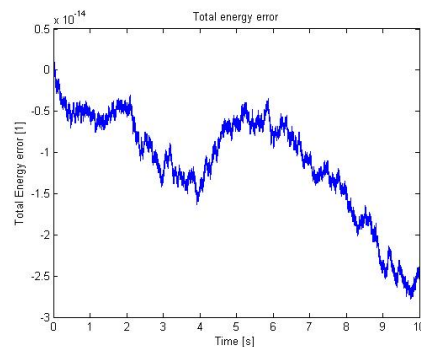
(c) Angle  $\psi$



(d) Position of the centre of the skateboard



(e) Total mechanical energy

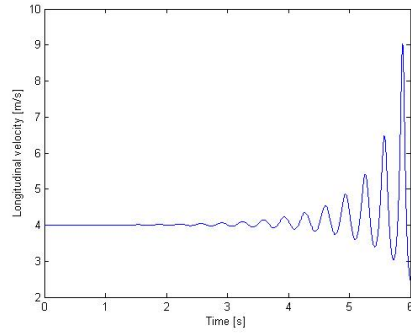


(f) Energy error

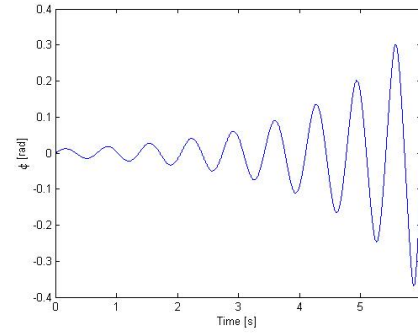
**Figure A.1:** Numerical simulations for totally self-balancing skateboard in the stable case

**Table A.2:** Values of parameters and initial conditions for totally self-balancing skateboard in dynamically unstable case

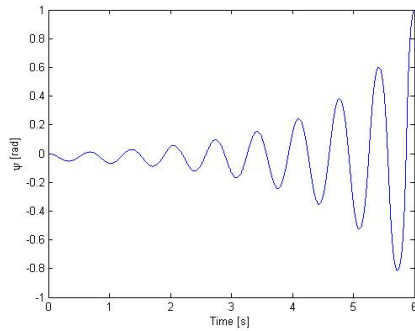
$s_t$	$a$	$\rho(0)$	$\sigma(0)$	$\varphi(0)$	$X(0)$	$Y(0)$	$\psi(0)$
[Nm]	[m]	[m/s]	[rad/s]	[rad]	[m]	[m]	[rad]
100	-0.05	4	0.1	0	0	0	0



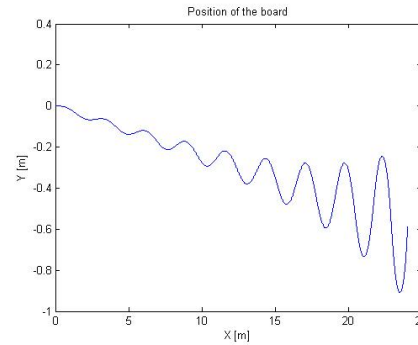
(a) Longitudinal velocity



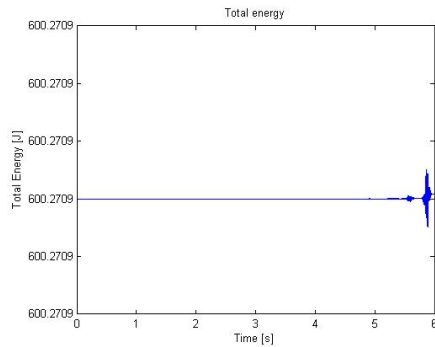
(b) Angle  $\varphi$



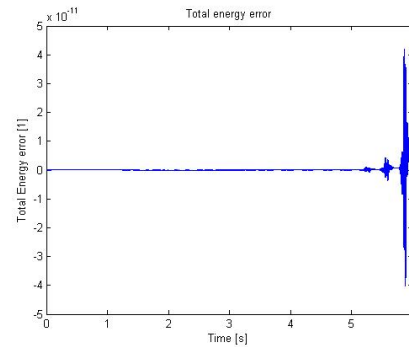
(c) Angle  $\psi$



(d) Position of the centre of the skateboard



(e) Total mechanical energy

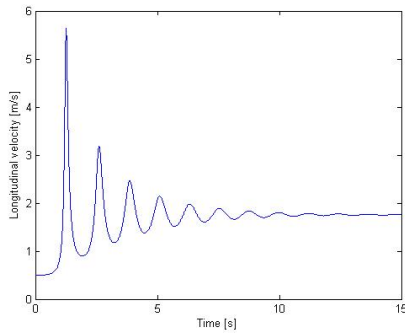


(f) Energy error

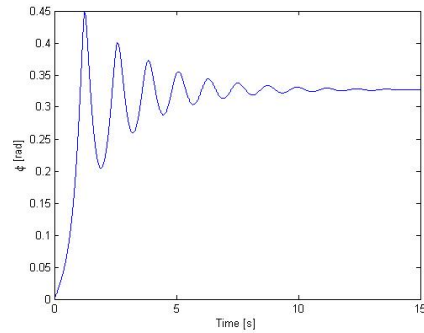
**Figure A.2:** Numerical simulations for totally self-balancing skateboard in dynamically unstable case

**Table A.3:** Values of parameters and initial conditions for totally self-balancing skateboard in the statically unstable case

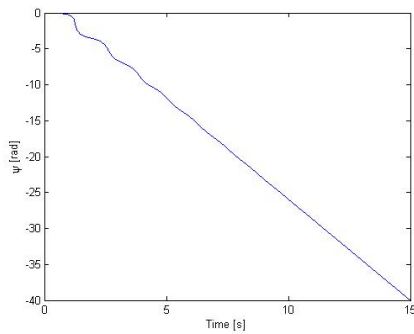
$s_t$	$a$	$\rho(0)$	$\sigma(0)$	$\varphi(0)$	$X(0)$	$Y(0)$	$\psi(0)$
[Nm]	[m]	[m/s]	[rad/s]	[rad]	[m]	[m]	[rad]
100	0.05	0.5	0.1	0	0	0	0



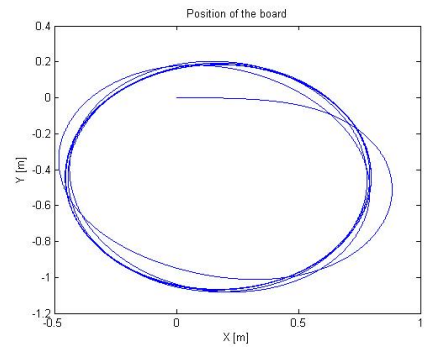
(a) Longitudinal velocity



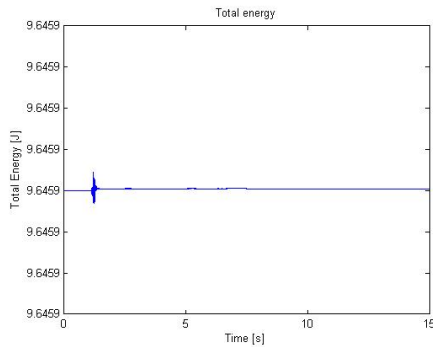
(b) Angle  $\varphi$



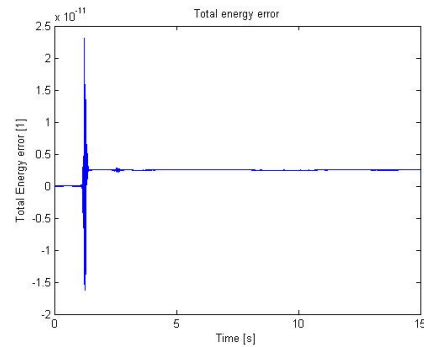
(c) Angle  $\psi$



(d) Position of the centre of the skateboard



(e) Total mechanical energy

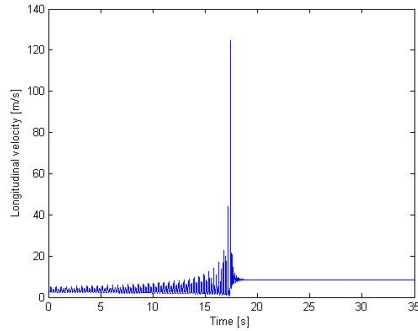


(f) Energy error

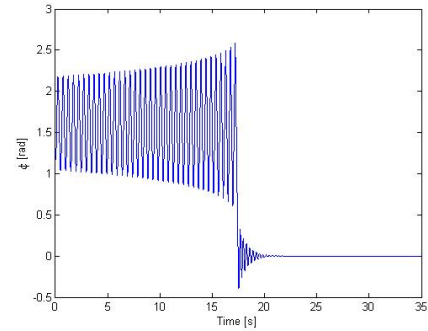
**Figure A.3:** Numerical simulations for totally self-balancing skateboard in the statically unstable case

**Table A.4:** Values of parameters and initial conditions for the totally self-balancing skateboard with large perturbation

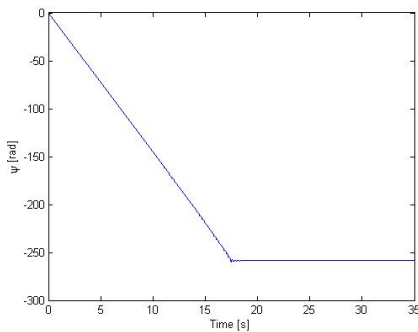
$s_t$	$a$	$\rho(0)$	$\sigma(0)$	$\varphi(0)$	$X(0)$	$Y(0)$	$\psi(0)$
[Nm]	[m]	[m/s]	[rad/s]	[rad]	[m]	[m]	[rad]
100	0.05	0.5	0	0	0	0	$\pi/3$



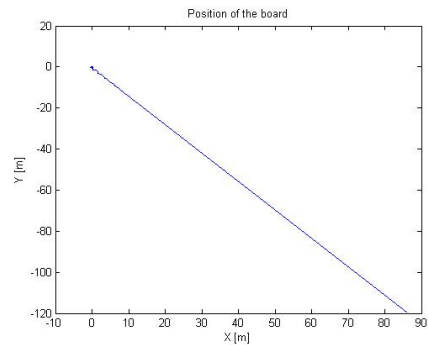
(a) Longitudinal velocity



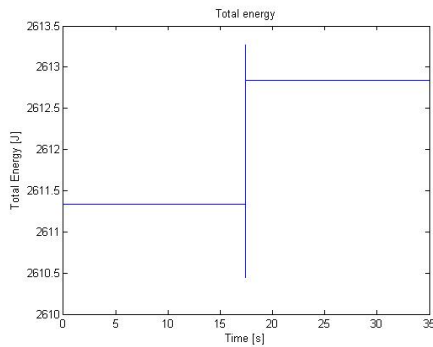
(b) Angle  $\varphi$



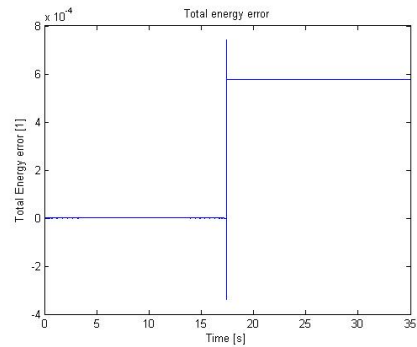
(c) Angle  $\psi$



(d) Position of the centre of the skateboard



(e) Total mechanical energy



(f) Energy error

**Figure A.4:** Numerical simulations for the totally self-balancing skateboard with large perturbation

# Appendix B

## Phase-space for the non-conservative skateboard model

Phase-space is more complicated in case when the parameter  $a$  is not zero as shown in Appendix B. They are computed numerically for negative and positive  $a$  with *Wolfram Mathematica* software with the same parameters as Figure 2.8.

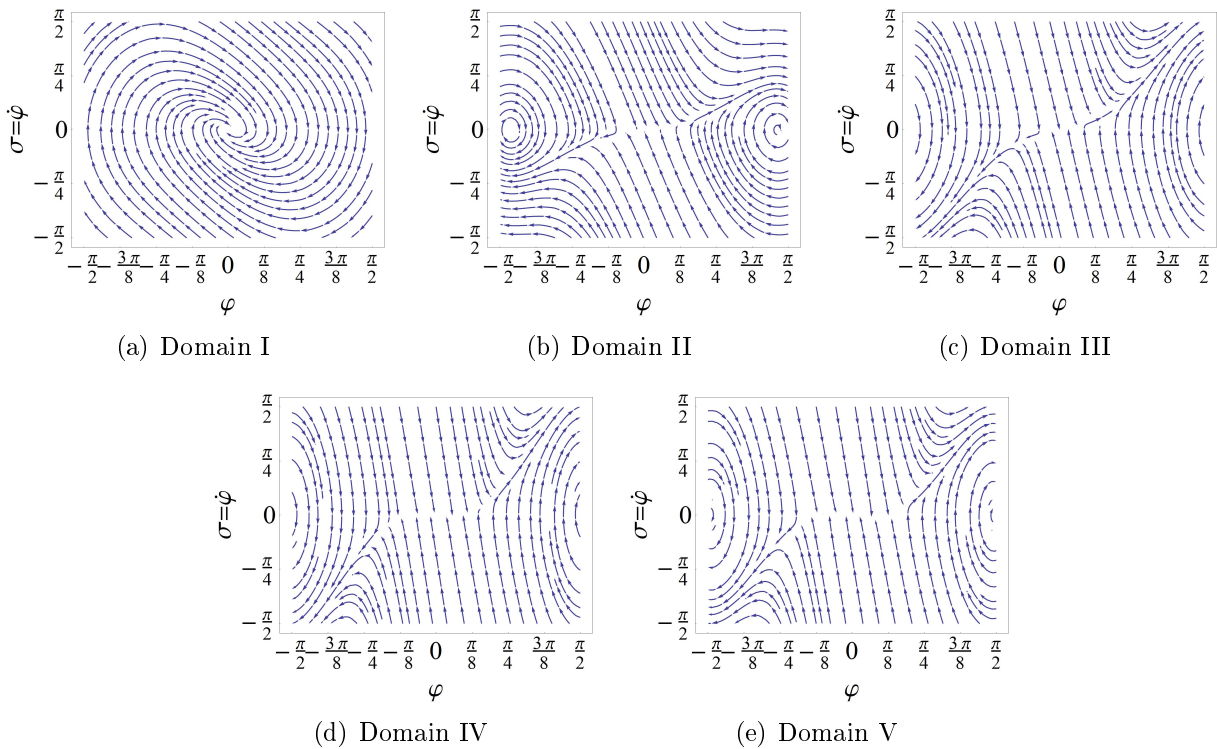


**Figure B.1:** Structure of phase-space for specific domains with a skater, who stands before the centre of the board

The equilibria are independent of the parameter  $a$ , so they are not changed in comparison with Figure 2.8. The centres become stable focus if  $a$  is greater than zero, and unstable focus if  $a$  is less than zero.

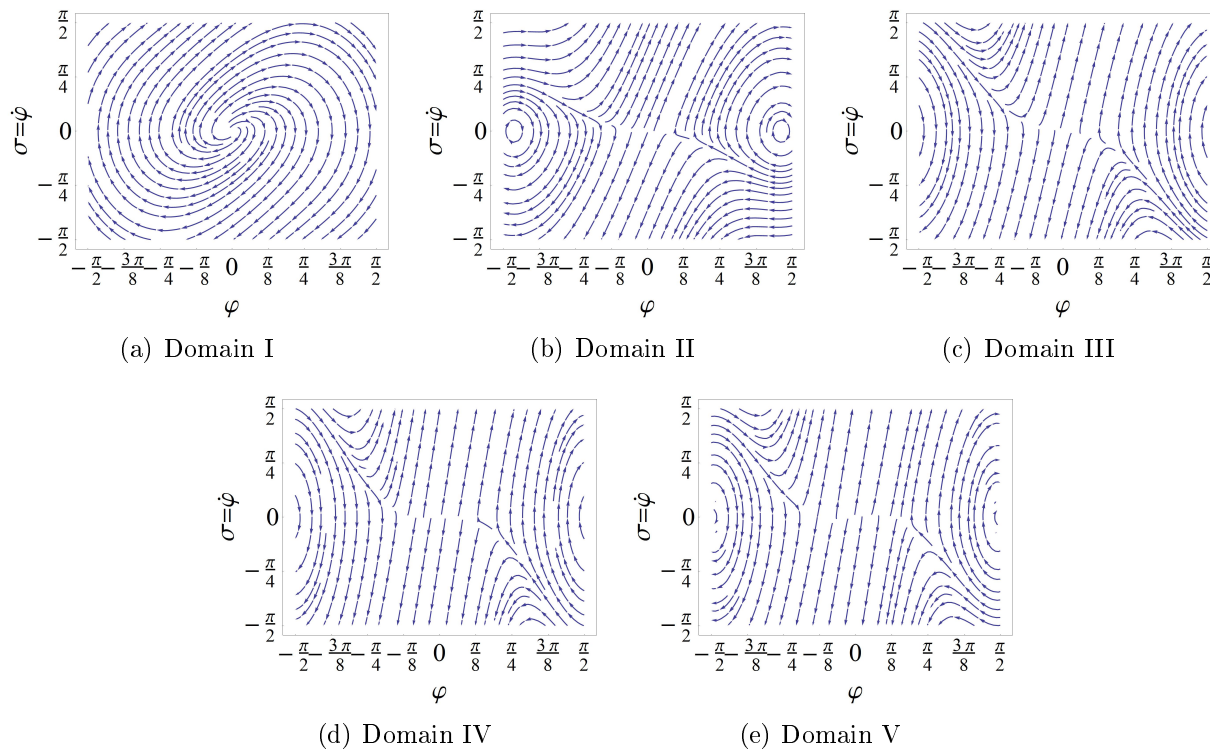


**Figure B.2:** Structure of phase-space for specific domains with a skater, who stands after the centre of the board

# Appendix C

## Numerical simulations for the nearly self-balancing skateboard

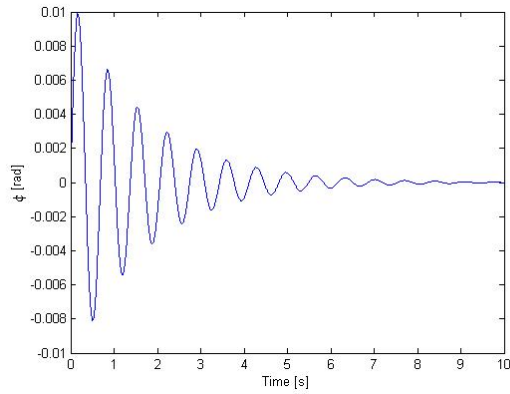
Numerical simulations for ordinary differential equation system (2.2.9) can be found in Appendix C. The numerical simulations is computed by the *ode45* function of MATLAB 2012b software.

The values used for the parameters, which are not the same for all simulations, can be found in the table before each numerical simulation. The other parameters are the same for every numerical solution and they can be found in Table 2.1. The energy error function can be computed as the same way as in Appendix A, expression (A.0.1).

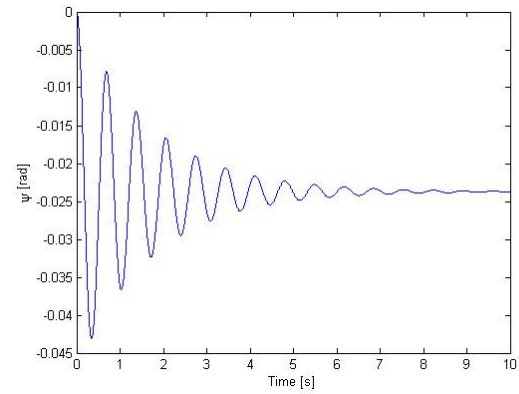
The simulation is unrealistic if  $|\varphi| > \pi/2$ , but it shows well the stability.

**Table C.1:** Values of parameters and initial conditions for nearly self-balancing skateboard in the stable case

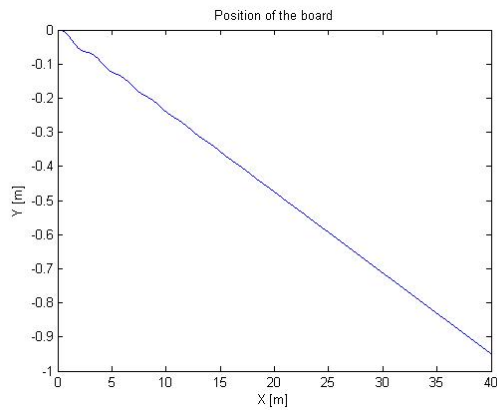
$s_t$	$a$	$V$	$\sigma(0)$	$\varphi(0)$	$X(0)$	$Y(0)$	$\psi(0)$
[Nm]	[m]	[m/s]	[rad/s]	[rad]	[m]	[m]	[rad]
100	0.05	4	0.1	0	0	0	0



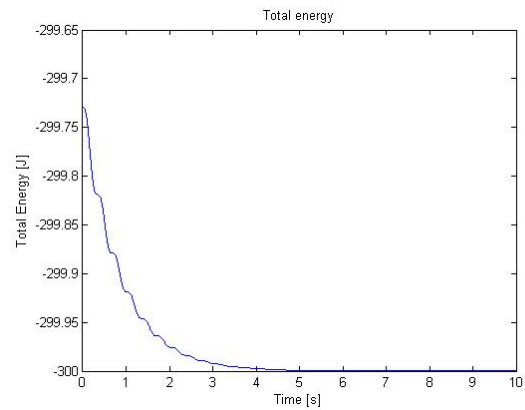
(a) Angle  $\varphi$



(b) Angle  $\psi$



(c) Position of the centre of the skateboard

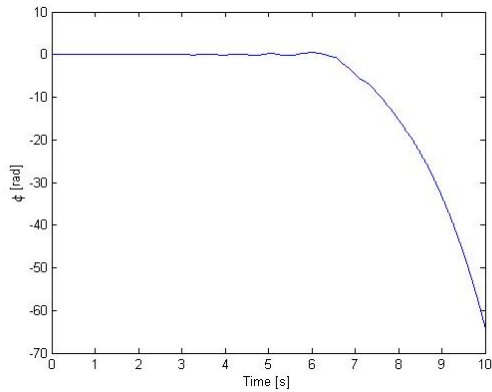


(d) Total mechanical energy

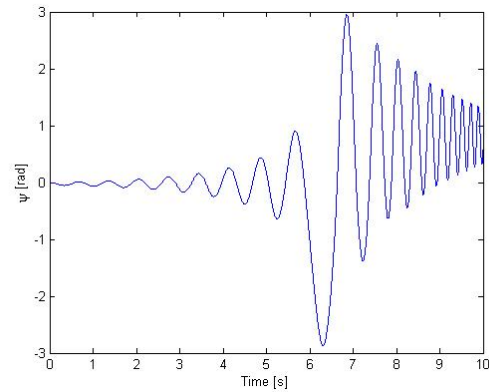
**Figure C.1:** Numerical simulations for nearly self-balancing skateboard in the stable case

**Table C.2:** Values of parameters and initial conditions for nearly self-balancing skateboard in the dynamically unstable case

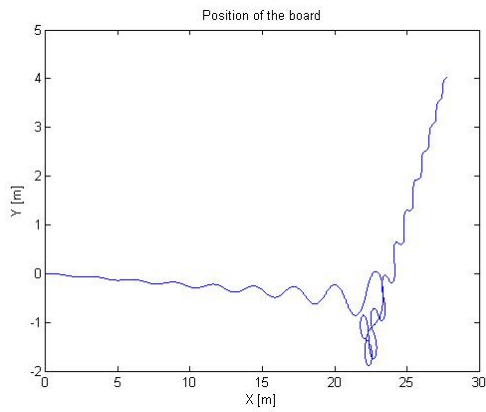
$s_t$	$a$	$V$	$\sigma(0)$	$\varphi(0)$	$X(0)$	$Y(0)$	$\psi(0)$
[Nm]	[m]	[m/s]	[rad/s]	[rad]	[m]	[m]	[rad]
100	-0.05	4	0.1	0	0	0	0



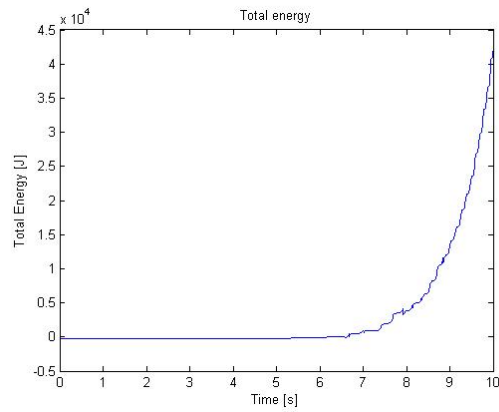
(a) Angle  $\varphi$



(b) Angle  $\psi$



(c) Position of the centre of the skateboard

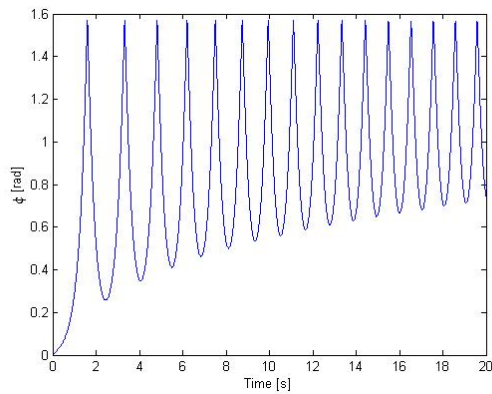


(d) Total mechanical energy

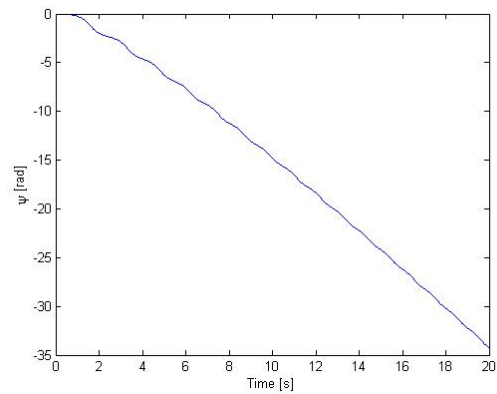
**Figure C.2:** Numerical simulations for nearly self-balancing skateboard in the dynamically unstable case

**Table C.3:** Values of parameters and initial conditions for nearly self-balancing skateboard in the statically unstable case

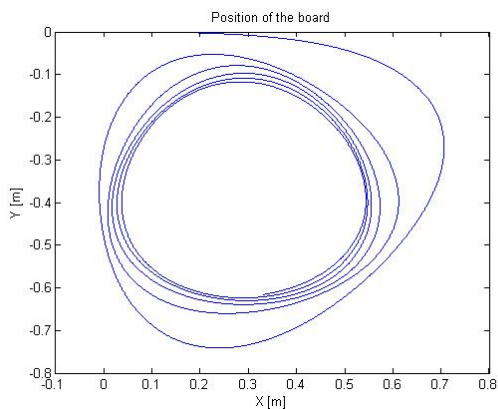
$s_t$	$a$	$V$	$\sigma(0)$	$\varphi(0)$	$X(0)$	$Y(0)$	$\psi(0)$
[Nm]	[m]	[m/s]	[rad/s]	[rad]	[m]	[m]	[rad]
100	0.05	0.5	0.1	0	0	0	0



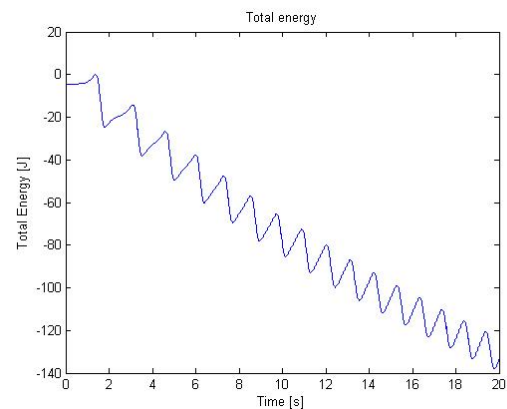
(a) Angle  $\varphi$



(b) Angle  $\psi$



(c) Position of the centre of the skateboard

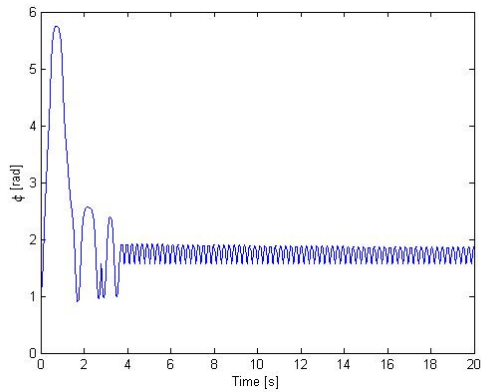


(d) Total mechanical energy

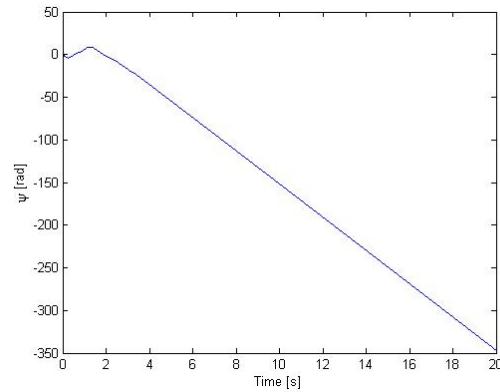
**Figure C.3:** Numerical simulations for nearly self-balancing skateboard in the statically unstable case

**Table C.4:** Values of parameters and initial conditions for nearly self-balancing skateboard with big perturbation

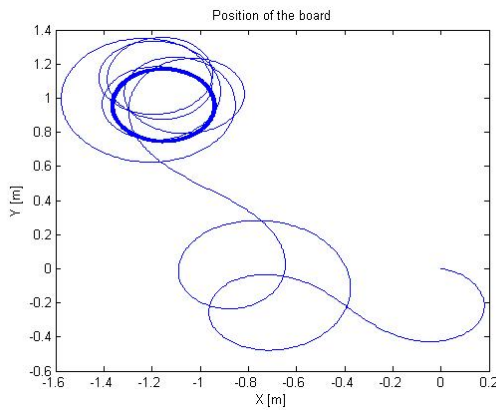
$s_t$	$a$	$V$	$\sigma(0)$	$\varphi(0)$	$X(0)$	$Y(0)$	$\psi(0)$
[Nm]	[m]	[m/s]	[rad/s]	[rad]	[m]	[m]	[rad]
100	0.05	0.5	0	0	0	0	$\pi/3$



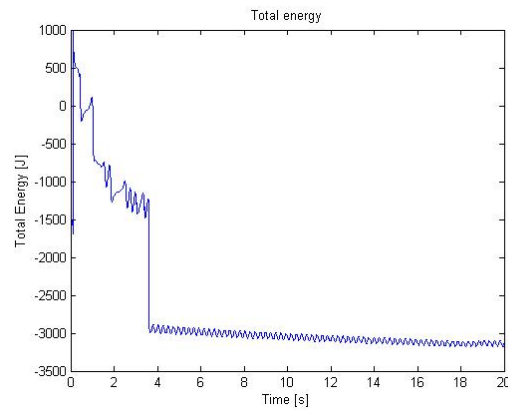
(a) Angle  $\varphi$



(b) Angle  $\psi$



(c) Position of the centre of the skateboard



(d) Total mechanical energy

**Figure C.4:** Numerical simulations for nearly self-balancing skateboard with big perturbation

# Appendix D

## Numerical simulations for the PD controlled skateboard

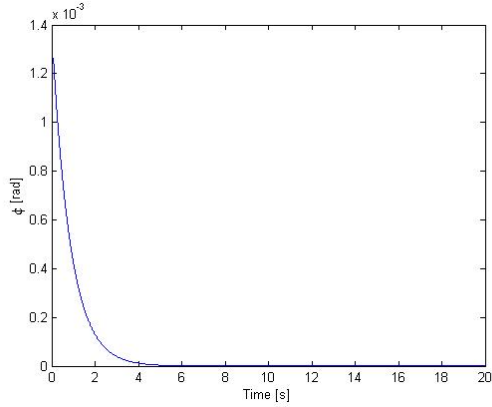
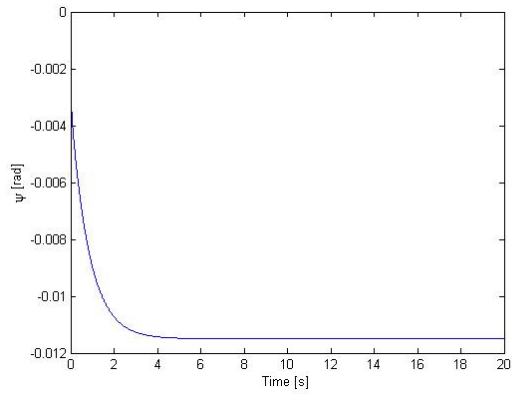
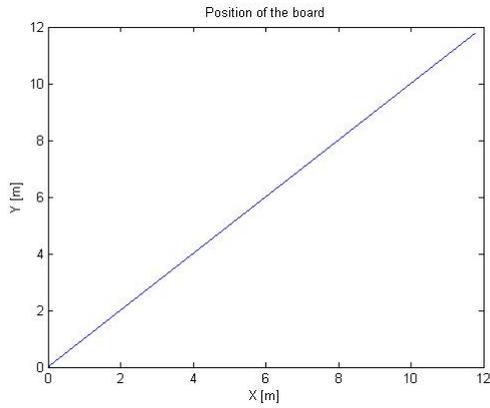
Numerical simulations for ordinary differential equation system (3.3.5) can be found in Appendix D. The numerical simulations is computed by the *ode45* function of MATLAB *2012b* software.

The values used for the parameters, which are not the same for all simulations, can be found in the table before each numerical simulation. The other parameters are the same for every numerical solution and they can be found in Table 2.1.

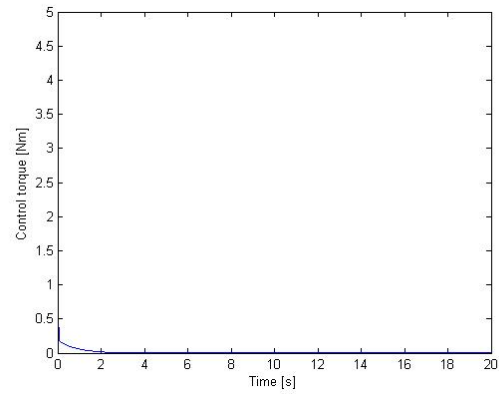
The simulation is unrealistic if  $|\varphi| > \pi/2$ , but it shows well the stability.

**Table D.1:** Values of parameters and initial conditions for PD controlled skateboard in the stable case with  $P$  less than  $P_c$  and negative  $a$

$P$	$D$	$s_t$	$a$	$V$	$\sigma(0)$	$\varphi(0)$	$X(0)$	$Y(0)$	$\psi(0)$
[Nm]	[Nms]	[Nm]	[m]	[m/s]	[rad/s]	[rad]	[m]	[m]	[rad]
200	50	50	-0.3	0.5	0.1	0	0	0	0

(a) Angle  $\varphi$ (b) Angle  $\psi$ 

(c) Position of the centre of the skateboard

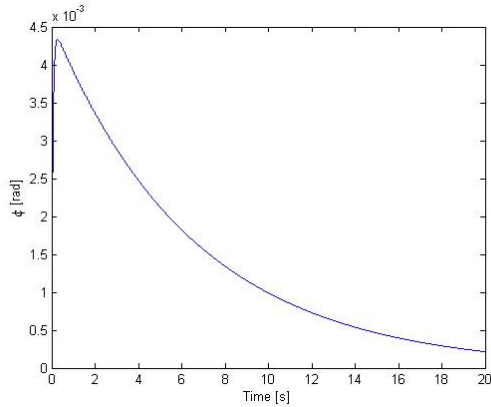
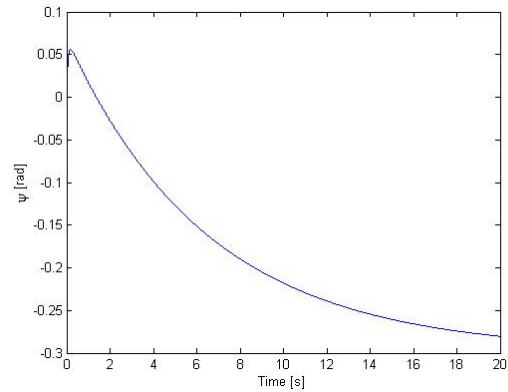
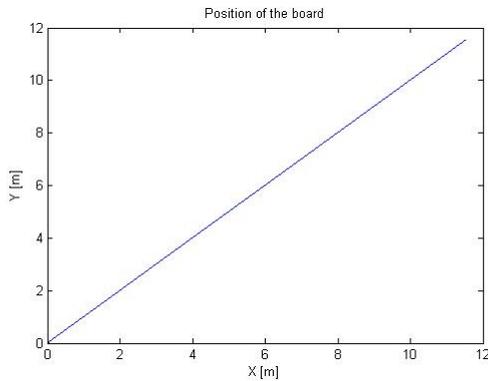


(d) Control torque

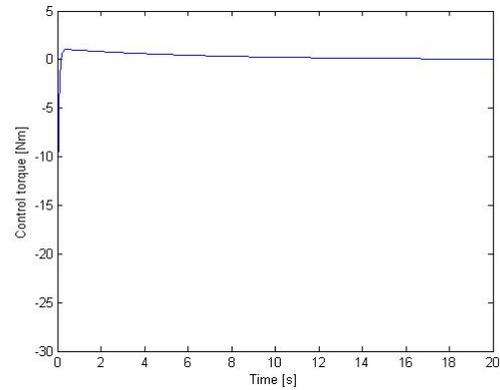
**Figure D.1:** Numerical simulations for PD controlled skateboard in the stable case with  $P$  less than  $P_c$  and negative  $a$

**Table D.2:** Values of parameters and initial conditions for PD controlled skateboard in the stable case with  $P$  less than  $P_c$  and positive  $a$

$P$	$D$	$s_t$	$a$	$V$	$\sigma(0)$	$\varphi(0)$	$X(0)$	$Y(0)$	$\psi(0)$
[Nm]	[Nms]	[Nm]	[m]	[m/s]	[rad/s]	[rad]	[m]	[m]	[rad]
200	-300	50	0.1	0.5	0.1	0	0	0	0

(a) Angle  $\varphi$ (b) Angle  $\psi$ 

(c) Position of the centre of the skateboard

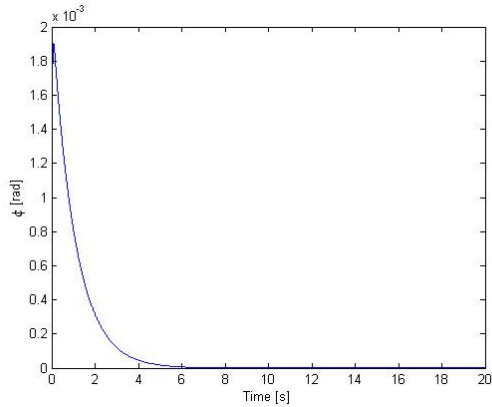
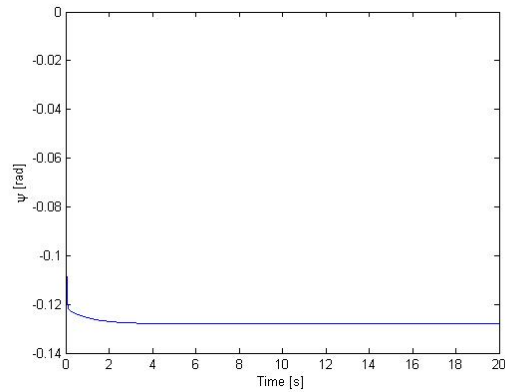
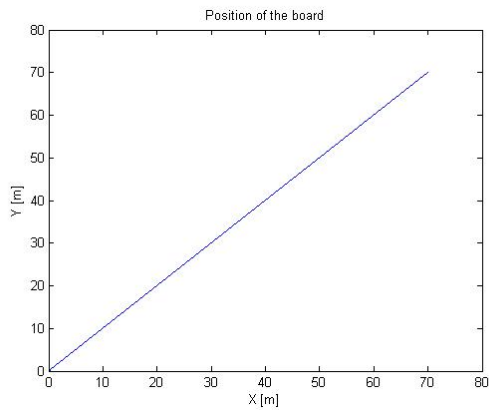


(d) Control torque

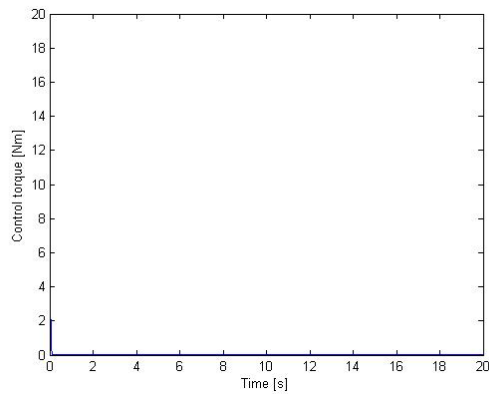
**Figure D.2:** Numerical simulations for PD controlled skateboard in the stable case with  $P$  less than  $P_c$  and positive  $a$

**Table D.3:** Values of parameters and initial conditions for PD controlled skateboard in the stable case with  $P$  more than  $P_c$

$P$	$D$	$s_t$	$a$	$V$	$\sigma(0)$	$\varphi(0)$	$X(0)$	$Y(0)$	$\psi(0)$
[Nm]	[Nms]	[Nm]	[m]	[m/s]	[rad/s]	[rad]	[m]	[m]	[rad]
200	200	50	0.05	3	0.1	0	0	0	0

(a) Angle  $\varphi$ (b) Angle  $\psi$ 

(c) Position of the centre of the skateboard

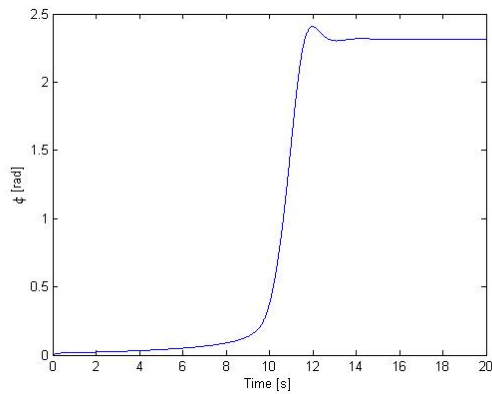
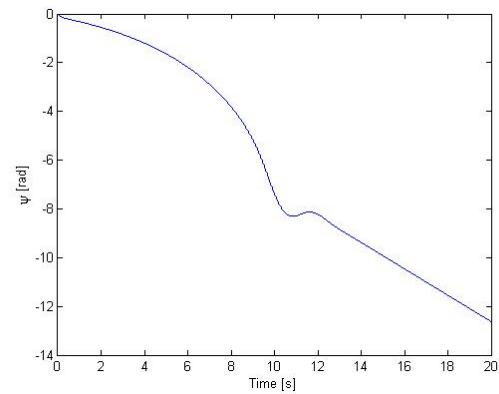
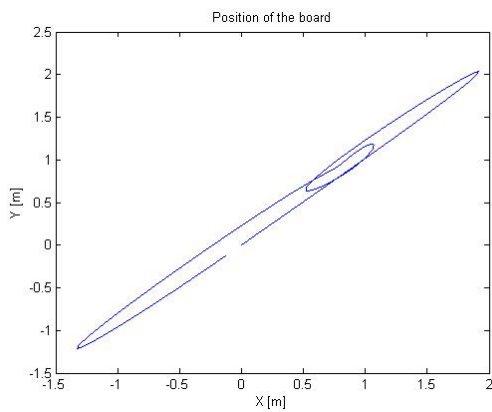


(d) Control torque

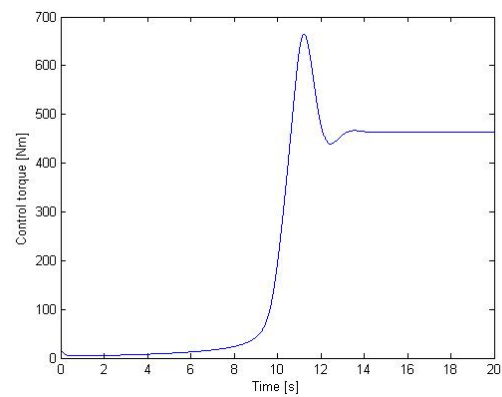
**Figure D.3:** Numerical simulations for PD controlled skateboard in the stable case with  $P$  more than  $P_c$

**Table D.4:** Values of parameters and initial conditions for PD controlled skateboard in the unstable case with  $P$  less than  $P_c$

$P$	$D$	$s_t$	$a$	$V$	$\sigma(0)$	$\varphi(0)$	$X(0)$	$Y(0)$	$\psi(0)$
[Nm]	[Nms]	[Nm]	[m]	[m/s]	[rad/s]	[rad]	[m]	[m]	[rad]
200	200	50	0.05	0.5	0.1	0	0	0	0

(a) Angle  $\varphi$ (b) Angle  $\psi$ 

(c) Position of the centre of the skateboard

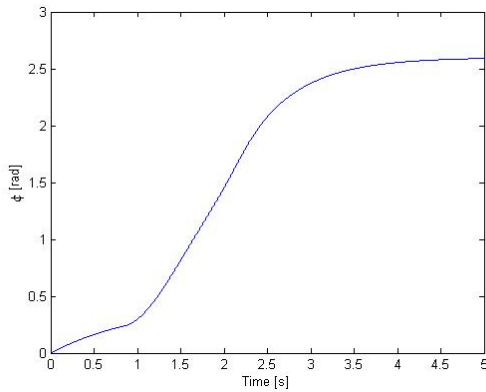


(d) Control torque

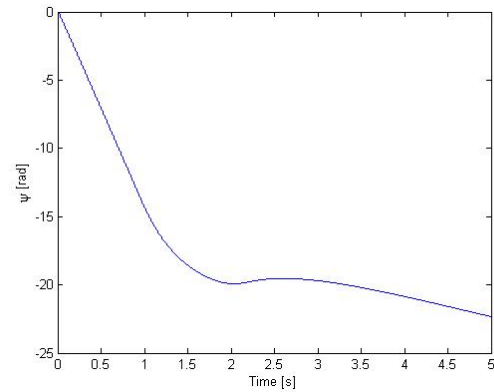
**Figure D.4:** Numerical simulations for PD controlled skateboard in the unstable case with  $P$  less than  $P_c$

**Table D.5:** Values of parameters and initial conditions for PD controlled skateboard in the unstable case with  $P$  more than  $P_c$

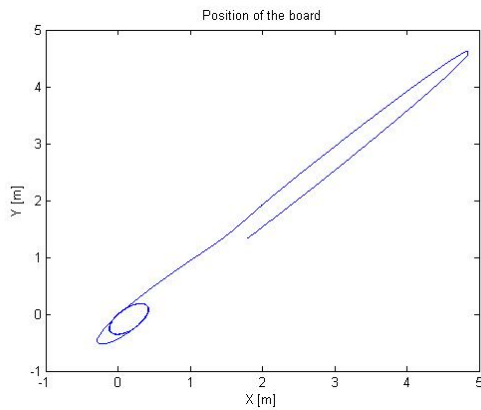
$P$	$D$	$s_t$	$a$	$V$	$\sigma(0)$	$\varphi(0)$	$X(0)$	$Y(0)$	$\psi(0)$
[Nm]	[Nms]	[Nm]	[m]	[m/s]	[rad/s]	[rad]	[m]	[m]	[rad]
200	200	50	-0.1	3	0.1	0	0	0	0



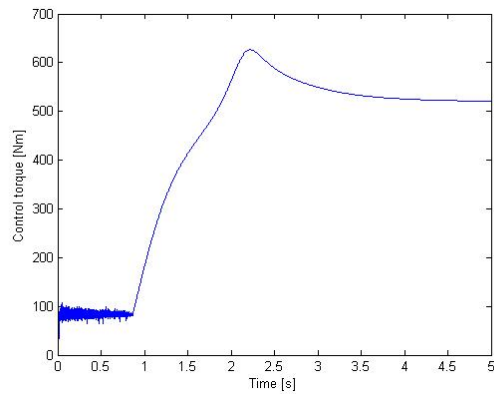
(a) Angle  $\varphi$



(b) Angle  $\psi$



(c) Position of the centre of the skateboard



(d) Control torque

**Figure D.5:** Numerical simulations for PD controlled skateboard in the unstable case with  $P$  more than  $P_c$

# Appendix E

## Numerical simulations for the delayed PD controlled skateboard

Numerical simulations for ordinary differential equation system (3.4.3) can be found in Appendix E. The numerical simulations is computed by the *NDSolve* function of *Mathematica* software.

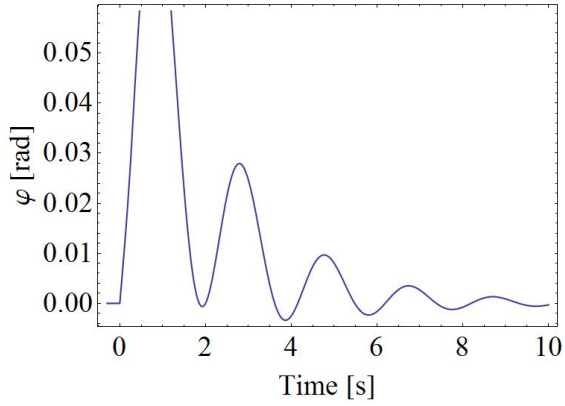
The values used for the parameters, which are not the same for all simulations, can be found in the table before each numerical simulation. The other parameters are the same for every numerical solution and they can be found in Table 2.1. The initial conditions are zero for all variables except  $X$ ; when  $t$  is less than zero, the initial data for  $X$  is

$$X(t < 0) = Vt. \tag{E.0.1}$$

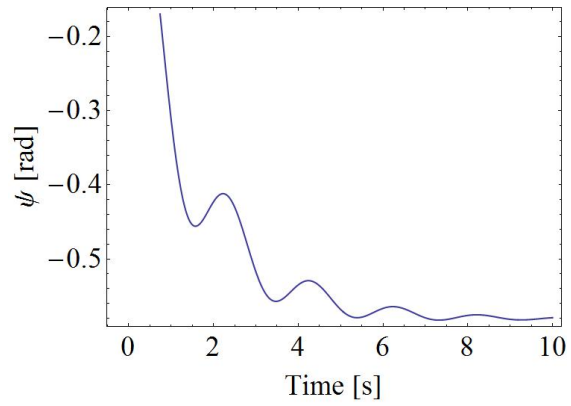
The simulation is unrealistic if  $|\varphi| > \pi/2$ , but it shows well the stability.

**Table E.1:** Values of parameters and initial conditions for delayed PD controlled skateboard for the stable case

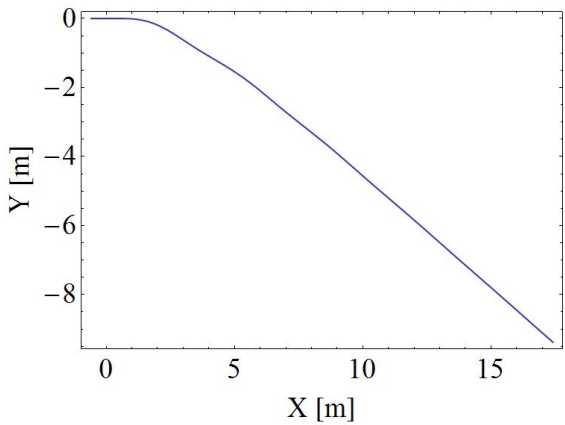
$P$	$D$	$\tau$	$s_t$	$a$	$V$	$\sigma(0)$	$\varphi(0)$	$X(0)$	$Y(0)$	$\psi(0)$
[Nm]	[Nms]	[s]	[Nm]	[m]	[m/s]	[rad/s]	[rad]	[m]	[m]	[rad]
50	20	0.294	100	0.05	2	0.1	0	0	0	0



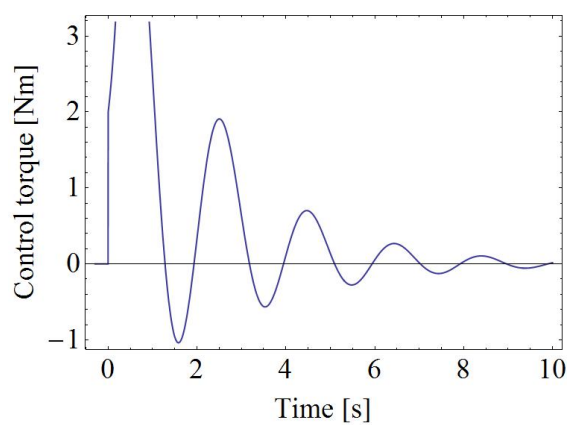
(a) Angle  $\varphi$



(b) Angle  $\psi$



(c) Position of the centre of the skateboard



(d) Control torque

**Figure E.1:** Numerical simulations for delayed PD controlled skateboard for the stable case

**Table E.2:** Values of parameters and initial conditions for delayed PD controlled skateboard for the statically unstable case

$P$	$D$	$\tau$	$s_t$	$a$	$V$	$\sigma(0)$	$\varphi(0)$	$X(0)$	$Y(0)$	$\psi(0)$
[Nm]	[Nms]	[s]	[Nm]	[m]	[m/s]	[rad/s]	[rad]	[m]	[m]	[rad]
46	20	0.294	100	0.05	2	0.1	0	0	0	0

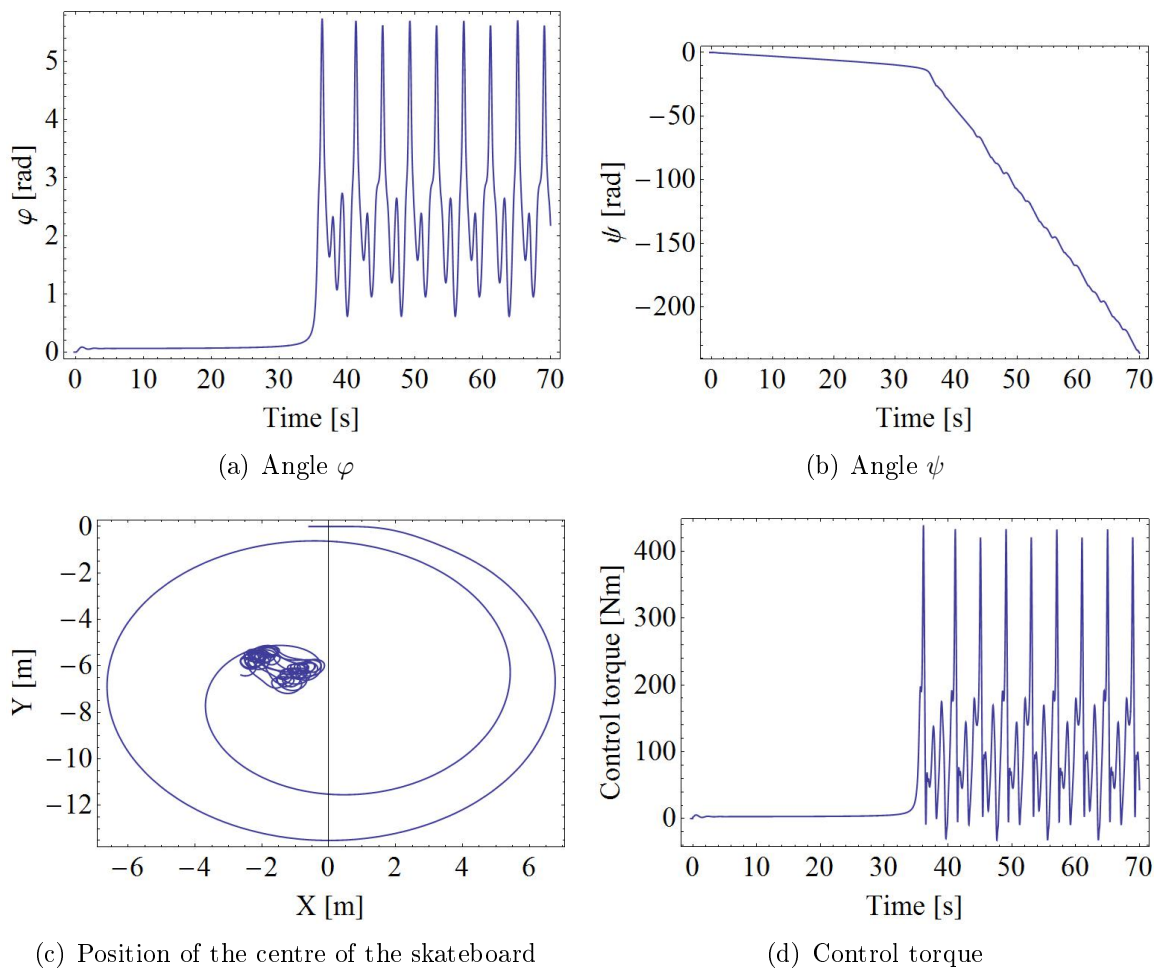


**Figure E.2:** Numerical simulations for delayed PD controlled skateboard for the statically unstable case

**Table E.3:** Values of parameters and initial conditions for delayed PD controlled skateboard for the statically unstable case at low speed

$P$	$D$	$\tau$	$s_t$	$a$	$V$	$\sigma(0)$	$\varphi(0)$	$X(0)$	$Y(0)$	$\psi(0)$
[Nm]	[Nms]	[s]	[Nm]	[m]	[m/s]	[rad/s]	[rad]	[m]	[m]	[rad]
600	220	0.294	100	0.05	0.105	0.1	0	0	0	0

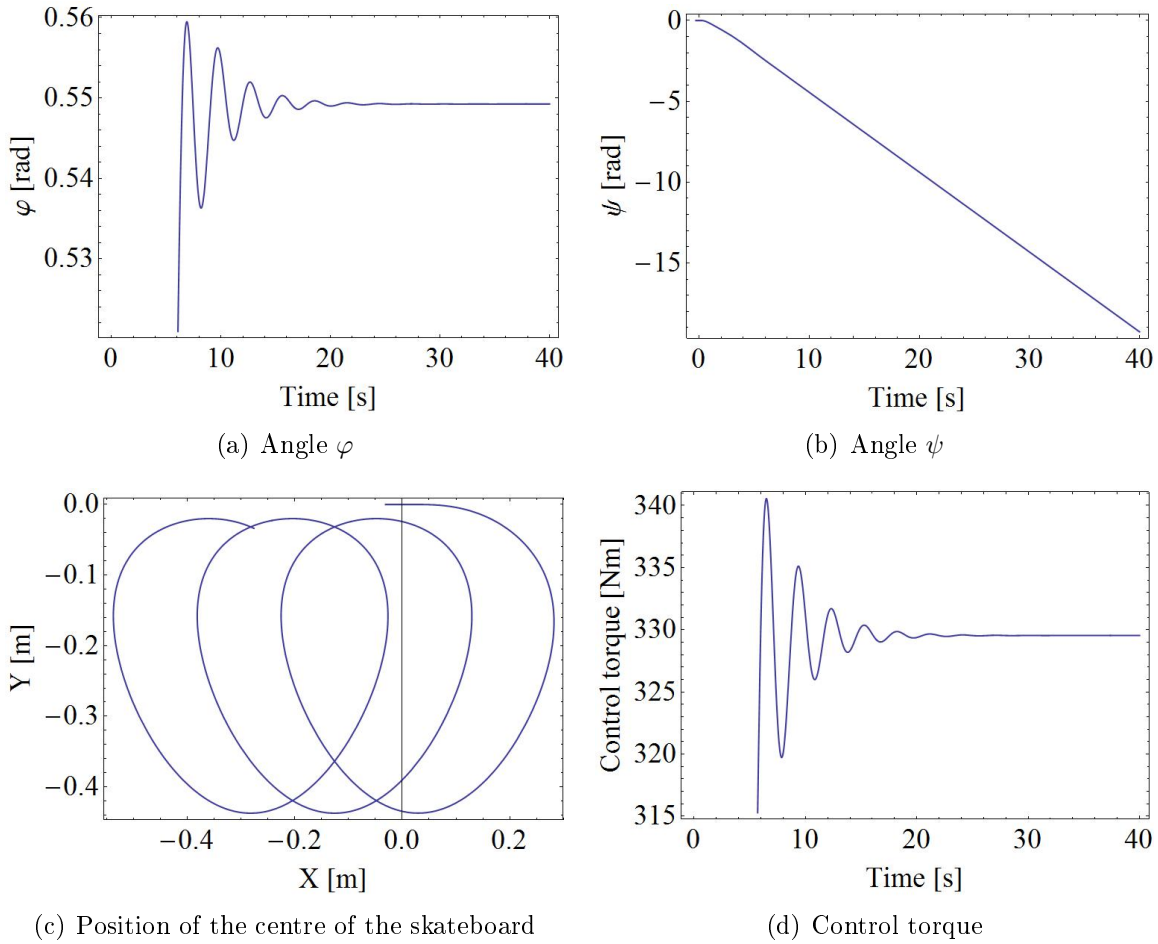


**Figure E.3:** Numerical simulations for delayed PD controlled skateboard for the statically unstable case at low speed

**Table E.4:** Values of parameters and initial conditions for delayed PD controlled skateboard for the dynamically unstable case

$P$	$D$	$\tau$	$s_t$	$a$	$V$	$\sigma(0)$	$\varphi(0)$	$X(0)$	$Y(0)$	$\psi(0)$
[Nm]	[Nms]	[s]	[Nm]	[m]	[m/s]	[rad/s]	[rad]	[m]	[m]	[rad]
60	20	0.294	100	0.05	2	0.1	0	0	0	0

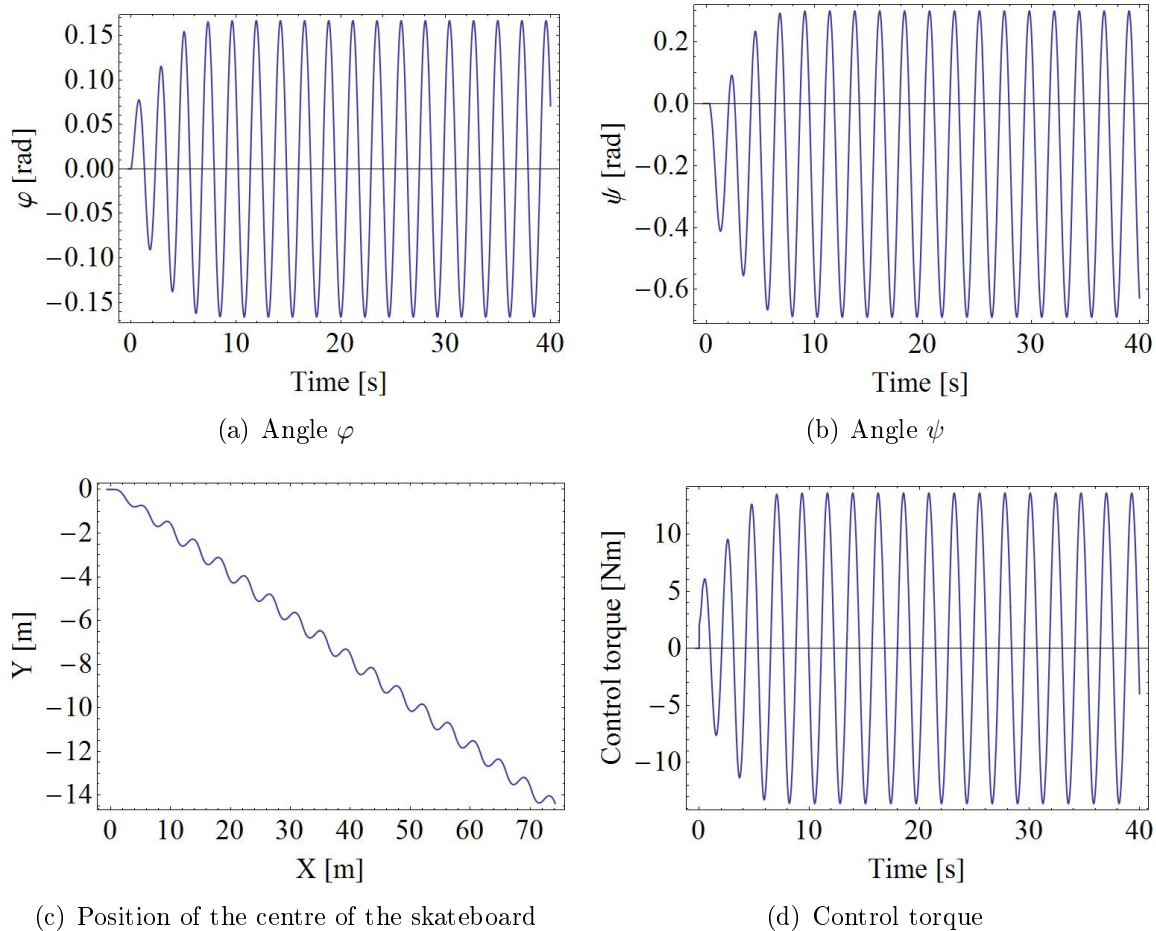


**Figure E.4:** Numerical simulations for delayed PD controlled skateboard for the dynamically unstable case